1-1-1978

Crack initiation and propagation in VAN-80 steel.

Brian L. Braglia

CRACK INITIATION AND PROPAGATION IN VAN-80 STEEL

by

Brian L. Braglia

A Thesis

Presented to the Graduate Committee

of Lehigh University

in Candidacy for the Degree of

Master of Science

in

Metallurgy and Materials Science

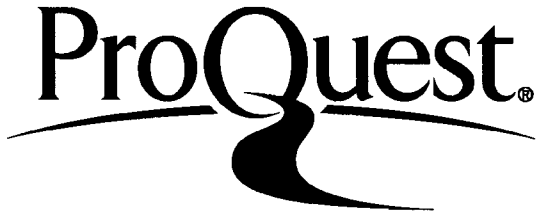

This thesis is accepted and approved in partial fulfillment of the requirements for the degree of Master of Science

February 8, 1978

Professor in Charge

Chairman of Department

ACKNOWLEDGEMENTS

At this time the author would like to express his appreciation to certain individuals and organizations who have afforded advice, assistance, and moral support during the course of this investigation:

To Professor Richard W. Hertzberg for advice, direction, and constructive criticism in his capacity as thesis advisor; To all the people in the machine shop for their part in preparing fatigue test specimens; To the Electro-Motive Division of General Motors for the fellowship which enabled me to spend the year at Lehigh, for performing chemical analyses of the subject steel, and for conducting surface roughness measurements on the polished test notches; To the Metallurgical Department secretary, Nancy Mikashus, for her excellent job in typing this thesis; To Jones and Laughlin Steel Company for supplying the VAN-80 used in the investigation and for determining the tensile properties of said steel; To the Pennsylvania Science and Engineering Foundation whose support under agreement 352 funded this investigation; To all my fellow graduate students for their help in making this entire year a very good time, especially during those official meetings of the von Laue Society. In particular, I would like to thank John Janiszewski, Phil Bretz,

and Mike Skibo for huge amounts of assistance and friendship given throughout the year.

TABLE OF CONTENTS

List of Figures and Tables

List of Tables

ABSTRACT

The fatigue crack initiation and propagation responses of a high strength low alloy steel, VAN-80, have been investigated. Crack propagation results attest to the isotropy of the material when tested in L-T and T-L orientations. This is to be expected due to the beneficial effects of inclusion shape control. Crack growth rates are similar to rates for normal ferrite-pearlite steels tested in the L-T orientation.

Crack initiation was defined, for the purposes of this investigation, as the existence of a 0.25 mm long crack on either surface of a modified compact tension specimen. The parameter $\frac{\Delta K}{\sqrt{\rho}}$ was used to normalize data concerning crack initiation at three finite radii notches (0.79, 1.59, and 3.18 mm). A volume effect on initiation was observed with larger radii producing shorter lives at a given $\frac{\Delta K}{\sqrt{\rho}}$. This volume control of the initiation process has also been reported by previous authors for many materials. The experimentally determined value of $\frac{\Delta K}{\sqrt{\rho}})TH$ for VAN-80 is 835 MPa. Samples cycled at or below this value would not be expected to initiate a crack in 10^6 cycles. Values of $\frac{\Delta K}{\sqrt{\rho}})TH$ for other engineering materials are often found in the range of 400-1000 MPa.

For all high block-low block tests, $\Sigma \frac{n}{N} > 1$. This by itself suggests that the total fatigue process is actually propagation controlled. However, the answer

has not proven to be so clear-cut. VAN-80 is highly sensitive to overload induced crack delay. Since the present definition of initiation contains a finite amount of propagation, delay effects may overshadow actual initiation.

TEM and SEM examinations of fracture surface micromorphology have determined that VAN-80 undergoes a fracture mechanism transition. A change from structure sensitive crack growth to structure insensitive crack growth occurs in the range 14-20 MPa$\sqrt{m}$. Fractography has also demonstrated that the ΔK level at short, newly initiated crack fronts is much lower than the externally applied ΔK level in the specimen. Finally, crack initiation occurred in notched VAN-80 samples by debonding of the globular cerium sulfides from the matrix at the surface of the notch root.

CRACK INITATION AND PROPAGATION IN VAN-80 STEEL

I. INTRODUCTION

1.1 HSLA Steel

In recent years a new category of steels has found wide acceptance where low cost, low weight, high strength, isotropic behavior in the as-rolled condition, and excellent weldability are important design criteria. This group is known collectively as high strength low alloy (HSLA) steels and VAN-80 is a well known member of the group.

Energy conservation is a necessity with known fuel reserves rapidly dwindling and, in the case of automobiles, efficiency standards have already been set by law. Auto, truck, rail, and off-road equipment will achieve this aim largely through weight reduction. HSLA steels allow weight reduction by reducing section thickness without sacrificing total component strength since these steels exhibit yield strengths two to three times higher than the steels being replaced. This is made possible without expensive alloying additions of chromium, nickel, molybdenum, etc. Instead, high strength is achieved in the as-rolled condition by ultra-small grain size, vanadium carbonitride precipitation strengthening, and manganese solid solution strengthening. Carbon levels are kept below 0.18%; thus, weldability of the HSLA steels is comparable to that of the plain, low carbon steels being replaced. Mechanical properties are

further enhanced through inclusion shape control; cerium additions to the melt form cerium sulfides which retain their globular shape during hot rolling operations.[1] This markedly reduces the anisotropy normally associated with ordinary hot-rolled products.

1.2 Crack Initiation & Propagation

Designing a structure to preclude failure during static loading is relatively straight forward,but few components are subjected solely to static loading. Failure due to cyclic or fatigue loading is then a major consideration. Two views of this problem can be taken; either one insures that a crack will not initiate during a component's service life or one insures that a crack once initiated will be detected before catastrophic failure occurs. In many industries (automotive in particular) the prevention of crack initiation is the main consideration. Most components designed with this objective in mind function as intended for their entire service life without cracking. Often, however, this is achieved by over-conservative design, i.e., by employing lower operating stresses and the attendant penalty of increased weight. Except in very redundant structures where load shifting is easily done, a crack,once initiated, will often proceed to final failure. Cracked parts are subject to warranty claims and may also be subject to government mandated recalls if safety is affected.

In addition, a serious loss of goodwill results due to repeated component failures during the expected service life.

If a crack does initiate it will usually occur in the vicinity of locally high stress fields such as at fillets, holes, corners, and welds or at service induced scratches, nicks, wear, and corrosion pits. In many cases it is not desirable to consider these notches as sharp cracks; doing so results in a very overconservative design situation with its attendant cost and weight penalties. Thus, it is highly advantageous to study crack initiation in the vicinity of notches.

While prevention of crack initiation may represent one design objective, knowledge of crack propagation is also useful. Many real life structures contain cracks and some very sharp notches are indeed crack-like. In these situations, crack growth rate information is useful to establish safe operating stress levels and adequate inspection intervals.

1.3 Previous Investigations

Other investigators have addressed themselves to these same questions with regard to other materials. Jack and Price[2] studied crack initiation at notches in plain low carbon steel plates. Their studies were confined to sharp notches with radii of 0.05 - 1.25 mm. Notches with radii less than 0.25 mm showed the

same initiation lives as did the 0.25 mm radius at any given applied stress level. For notches with radii from 0.25 - 1.25 mm the applied stress required for crack initiation at a given number of cycles increased with the notch radius. They proposed that a parameter $\frac{\Delta K}{\sqrt{\rho}}$, where ΔK is the stress intensity range and ρ is the notch radius, be used to analyze the data. This parameter is actually a representation of the stress at the surface of the notch. Barsom and McNicol[3] then used this approach in their study of crack initiation of HY-130 steel. The parameter, $\Delta K/\sqrt{\rho}$, was found to normalize all initiation data from notches with radii of 0.20 - 9.53 mm. A slight volume effect was seen with larger radii producing shorter lives at a given $\Delta K/\sqrt{\rho}$ level. It may be reasoned that when the notch radius is increased, a greater volume of material is subjected to high stress at the notch root. Consequently, fatigue life would be expected to be shorter since the probability of having a crack initiation site in the larger critical zone would be greater. Clark[4] also used the same approach in his examination of the crack initition behavior of type 403 stainless steel. While the two previously mentioned investigations used single-edge or double-edge notch samples, Clark used the compact tension configuraton. Forman[5] looked at initiation from flaws of varying root radii (0.025 - 3.18 mm) in 7075-T6 aluminum, but did not employ the parameter

$\frac{\Delta K}{\sqrt{\rho}}$ to analyze the data. Instead, the ratio $\frac{K_{max}}{K_a}$ was used, where Ka is the critical stress intensity for fast fracture at a given finite notch radius. Since Ka depends on ρ, this parameter is similar to the one discussed above. Another approach to the same problem has been attempted by Morrow, Lawrence, and others at the University of Illinois[6]. They first define the cyclic properties of a material and then use a finite element analysis to describe the state of stress at the given notch configuration. Use of a computer model and cycle by cycle damage summation then allow for the prediction of crack initiation life at the notch.

The fracture toughness and crack propagation behavior of VAN-80 have previously been examined[1]. The marked isotropy of the material was evident with regard to both properties. It was also shown that VAN-80 forms well defined striations on the fracture surface at intermediate levels of ΔK.

Other investigators[7-11] have characterized fracture surface micromorphology in normal ferrite-pearlite steels. These steels, as a group, tend to exhibit a transition from structure sensitive crack propagation (characterized by intergranular failure) at low ΔK levels, to structure insensitive propagation (characterized by striation formation) at intermediate ΔK levels. A similar transition has also been noted in non-ferrous alloys. Hertz-

berg and Mills[12] characterized the fracture surface micromorphology of several FCC and HCP materials and found the occurance of faceting, another structure sensitive process, at low ΔK levels in these materials.

1.4 Objectives

Thus, the basic objectives of this thesis will be as follows:

1. To develop S-N type crack initiation data for notched samples of VAN-80, containing different notch radii.
2. To investigate the effects of deliberate overloads on crack initiation in notched VAN-80 samples.
3. To determine crack propagation behavior ($\frac{da}{dn}$ VS ΔK) of the present supply of VAN-80 and to compare this with previous data.
4. To define low growth rate fracture surface micromorphology for the present VAN-80 and the previous supply of VAN-80.
5. To examine fracture surfaces generated during the crack initiation study and to characterize fracture surface micromorphology at short crack lengths in terms of known VAN-80 FCP micromorphology.

II. EXPERIMENTAL PROCEDURES

2.1 Materials

The material used in this study was VAN-80 produced by Jones and Laughlin Steel Company in conformance with ASTM A-656-72a grade 1 requirements. The steel sheet used for the crack initiation and propagation work was supplied in 1.4 m widths with a thickness of 4.62 mm. In addition, metallographic and fractographic examinations were conducted on 7.87 mm thick crack propagation specimens previously tested by Hertzberg and Goodenow.

2.2 Tensile Properties, Chemical Analysis, and Optical Metallography

Standard tensile properties (yield strength, ultimate tensile strength, uniform elongation, and total elongation) of the subject VAN-80 were measured by personnel at Jones and Laughlin's research laboratories. Hardness measurements were taken on the B and C scales of a Rockwell hardness tester.

Chemical analysis of the steel was performed in the Materials Laboratory of the Electro-Motive Division of General Motors Corporation. The carbon, phosphorus, sulfur, manganese, vanadium, nickel, aluminum, chromium, and molybdenum contents were determined. In addition, a fellow graduate student, Mr. A. D. Romig, analyzed sulfide inclusions and microstructural bands in the VAN-80 with the aid of an electron microprobe.

Samples oriented longitudinal and transverse to the rolling direction from both the new VAN-80 (4.62 mm thick) and old VAN-80 (7.87 mm thick) material supply were prepared for metallographic observation. Final polishing was accomplished using Linde B abrasive (.03 micron) and etching was done in a 2% nital solution.

2.3 Specimen Preparation

A modified compact tension configuration was used for crack initiation tests. The normal V-notch was replaced by a finite radius notch (Fig. 1); the ratio of "crack" length to specimen width was set at 0.5 ($\frac{a}{w} = 0.5$). Crack length was defined as the distance from the load line to the notch root. Three finite radii were tested--0.79, 1.59, and 3.18 mm (Fig. 2). After final machining operations, the sample thickness ranged from 4.29 to 4.44 mm. Notches were placed such that loading would always be parallel to the rolling direction.

The processing of these samples is quite important and therefore will be described in detail. The specimens were first machined to finished dimensions with the exception of the finite radius notch. The notch was then drilled at constant feed and speed in the presence of a cutting fluid. The hole was always drilled undersized by 0.40 mm. Using the same feeds and speeds, the holes were then reamed to final dimensions. At this point in time the oxide coating (mill scale) was removed from the

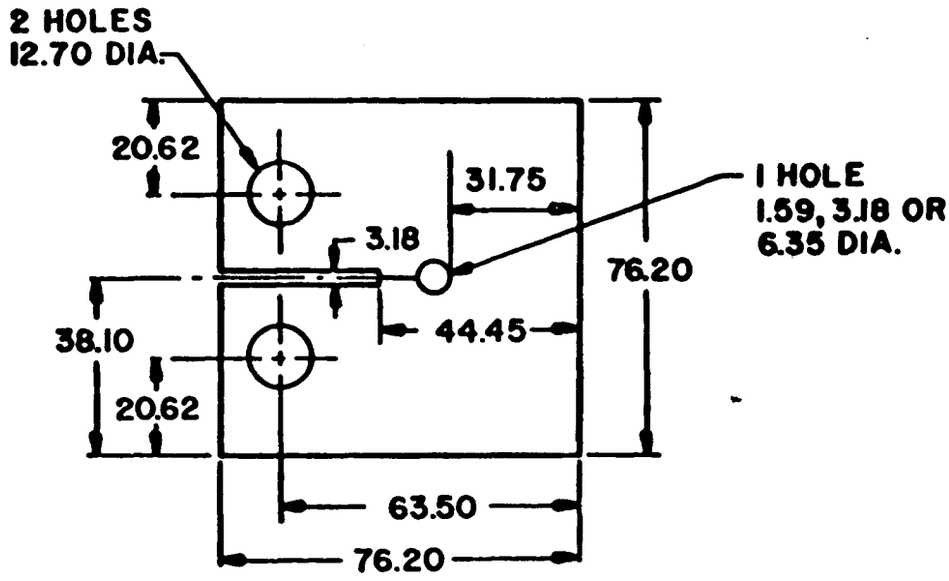

Fig. 1 Finite radius compact tension specimen.

Fig. 2 Modified compact tension samples containing the three sizes of finite notch radii.

sample by surface grinding; this also served to remove any burrs produced by drilling and reaming. Final polishing of the notch surface was achieved by coating wooden dowels with 6 micron diamond paste and rotating the dowels (with the aid of a drill press) within the reamed hole. All visible scratches were thus removed from the notch. Surface roughness measurements, made with the aid of a Tallysurf Profilometer, yielded a surface finish of 0.13μAA. After final polishing was completed, a jewelers saw was used to connect the previously machined slot with the carefully prepared hole.

Crack propagation tests were conducted on simple compact tension type specimens (Fig. 3). Notches were oriented both longitudinal and transverse to the rolling direction. Mill scale was removed on only one side of each sample to permit crack observation; thus, specimen thickness was 4.60 mm.

2.4 Crack Initiation Test Procedures

Fatigue crack initiation testing was carried out on 9KN and 90KN MTS electrohydraulic closed loop testing machines (Fig. 4). The higher capacity system was used for tests requiring loads in the range 9-18KN. All tests were run under load control at a frequency of 60 Hz with $\frac{Kmin}{Kmax} = .1$. Since the electronic control equipment was equipped with a peak load cutoff display oscilloscope, only the upper and lower 0.1% of the load

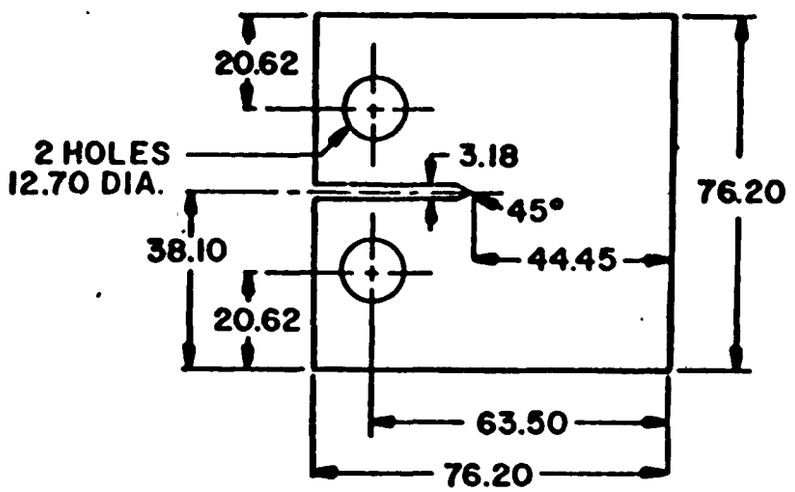

Fig. 3 Standard compact tension crack propagation specimen.

Fig. 4 MTS electro-hydraulic fatigue test equipment.

range was displayed on the oscilloscope. This allowed for very accurate control of the imposed loads.

Crack initiation throughout the study was defined to be the development of a 0.25 mm long crack, visible on either surface of the specimen. Due to the excellent finish produced by surface grinding, cracks of this length were easily visible to the naked eye. However, other more sophisticated means of crack detection were also employed. When a crack initiates, the compliance of the specimen increases. The MTS equipment is subsequently forced to provide a longer stroke to supply the same load as for an uncracked sample. At 60 Hz, however, this is not totally possible due to limitations of the test machine response. Consequently, the load drops very slightly (0.02 - 0.05% of total load). Due to the previously mentioned peak load cutoff display on the oscilloscope, this small change in loading is immediately evident to the experimenter. Existence of a crack is then confirmed visually, both with the naked eye and with the assistance of a 50X Gaertner travelling microscope which was also used to precisely measure crack length. If no crack could be detected after one million cycles, the test was stopped and the sample considered to be a run-out. After a crack had initiated, it was allowed to grow for several millimeters to obtain crack propagation data. During this subsequent propagation

stage, test frequency was reduced to 20 Hz.

2.5 Block Load Test Procedures

In these experiments, samples with finite notch radii of 1.59 and 3.18 mm and also samples containing sharp cracks ($\rho \rightarrow o$) were first subjected to a block of high loads. The high block loading sequence consisted of 1500 cycles at a load range which would be expected (from prior base-line data) to cause crack initiation (0.25 mm crack) in 3000 cycles. These overloads were applied at a frequency of 5 Hz. At this point, loads were decreased as desired, the frequency increased to 60 Hz, and cycling allowed to continue until crack initiation was observed. Percent overload $\left(\frac{\Delta K_{\text{high block}} - \Delta K_{\text{low block}}}{\Delta K_{\text{low block}}} \times 100\%\right)$ was thus varied from 20 to 120% depending on the choice of $\Delta K_{\text{low block}}$.

2.6 Crack Propagation Test Procedures

Loads were imposed such that the stress intensity range varied from 10 MPz$\sqrt{m}$ at the shortest crack length to greater than 90 MPa$\sqrt{m}$ near final fracture with $\frac{K_{min}}{K_{max}} = 0.1$ at all times. Test frequency was initially set at 60 Hz. As sample compliance increased, the frequency was lowered successively to 40, 20, 10, and 5 Hz. Crack advance was measured periodically with a 50X travelling microscope. The number of cycles between successive measurements was varied such that $\Delta a \leq 0.25$ mm.

A computer program was then used to reduce the data with output giving values of ΔK and $\frac{da}{dn}$.

Crack growth rate was calculated by the method:

$$\left(\frac{da}{dn}\right)_{a_i} = \frac{a_{i+1} - a_{i-1}}{n_{i+1} \quad n_{i-1}} \qquad (1)$$

A plastic zone size correction of the crack length, based on a state of plane stress, was incorporated into the program. The program also supplied a least squares fit of the data to Paris' crack growth rate equation

$$\frac{da}{dn} = C\Delta K^m \qquad (2)$$

which is a linear relationship when plotted on log-log coordinates.

2.7 Fractography

Transmission electron microscopy (TEM) was used to characterize fracture surface micromorphology of samples generated during crack initiation and crack propagation studies. Also, crack propagation specimens previously tested by Hertzberg and Goodenow were examined in this manner. Two stage platinum-carbon replicas were taken from samples of interest. For crack initiation samples, two replicas each 2.2 X 1.5 mm were taken from each specimen in the vicinity of the initiation site. For studies of crack propagation, approximately ten replicas, each 2.2 X 1.5 mm, were taken from each fracture surface. Every replica therefore spanned an applied stress intensity factor range of 1 - 3 MPa$\sqrt{m}$ depending upon the

crack size and associated ΔK gradient. A major portion of the fractographic study was conducted on a Phillips 300 transmission electron microscope which was operated at an accelerating potential of 60 KV. This microscope allowed for excellent resolution and observations were routinely made at magnifications up to 54000X; the instrument also has a goniometer stage which enabled the viewer to get a much more accurate idea of fracture surface topography. Much data at magnifications up to 39000X was also obtained on a RCA EMU-3G transmission microscope.

In addition to the TEM procedures just described, scanning electron microscopy (SEM) was used to examine several crack iniation specimens. No special preparation of the fracture surfaces was necessary before examination in the Etec Autoscan unit. A magnification of 20,000X proved to be the limit for practical observation on this instrument. The Etec unit was also equipped for microprobe analysis which allowed for a qualitative local chemical analysis of any feature on the fracture surface.

III. PRESENTATION AND DISCUSSION OF RESULTS

3.1 Results of Chemical Analyses, Tensile Tests, and Optical Microscopy

Results of chemical analyses performed on VAN-80 steel used in this investigation (supply A) are presented in Table I along with the chemical specifications for ASTM A-656-72a, Grade 1 steel. In addition, the chemical analysis is given for the VAN-80 steel used by Hertzberg and Goodenow (supply B) in previous crack propagation tests.[1]

Both supplies of VAN-80 meet chemical specifications as set forth by ASTM. Cerium is added to VAN-80 in very small amounts to combine with sulfur to bring about inclusion shape control. Electron microprobe analyses of supply A confirmed the presence of cerium sulfides which contained little iron and manganese.

Results of standard tensile tests on the subject VAN-80 are presented in Table II. Tensile properties, both longitudinal and transverse to the rolling direction, were determined for supply A. Again, ASTM specifications and results for supply B are included for comparison.

Isotropy, as provided by inclusion shape control, is apparent when longtudinal and transverse tensile properties of supply A are compared. Both supply A and supply B meet ASTM tensile requirements. However, supply A has a yield strength 14.6-18.4% higher than supply B

TABLE I: VAN-80 CHEMICAL ANALYSIS

	A-656, Grade 1 Spec.	VAN-80 Supply A	VAN-80[1] Supply B
Carbon	0.18 Max.	0.12	0.14
Manganese	1.60 Max.	1.43	1.36
Sulfur	0.050 Max.	0.007	0.007
Phosphorus	0.040 Max.	0.030	0.004
Silicon	0.60 Max.	0.48	0.56
Aluminum	0.02 Min.	0.02	0.064
Vanadium	0.05-0.15	0.125	0.10
Nitrogen	0.005-0.030	NA	0.017
Chromium		0.03	NA
Molybdenum		0.016	NA
Nickel		0.057	NA

NA = Not Available

TABLE II: VAN-80 MECHANICAL PROPERTIES

	A-656 Grade 1 Spec.	VAN-80 Supply A Longitudinal	VAN-80 Supply A Transverse	VAN-80[1] Supply B Longitudinal
Yield Strength (MPa)	552 Min.	634	655	553
Tensile Strength (MPa)	655-793	758	758	689
Total Elongation (%)	12 Min.	25	21.5	21
Uniform Elongation (%)		14.5	13.5	12.5
Hardness (R_c)		22	22	

tested by Hertzberg and Goodenow.[1] For this reason, fatigue crack propagation tests on supply A were included in this study to determine whether this moderate difference in yield strengths would affect crack propagation rates.

Several significant observations were made during metallographic observation of VAN-80 specimens. At low magnification (200X), distinct microstructural banding was seen in both longitudinal and transverse sections of supply A (Figures 5a, b). Since the bands are seen in both planes it was concluded that they were planar, rather than linear, features. Apparently, the bands had no effect on tensile properties (see Table II). Electron microprobe analysis of the bands revealed that they are manganese-rich areas of the steel.

High magnification (500X) photomicrographs of longitudinal and transverse sections of supply A (Figures 6a,b) allowed for easy estimation of grain size. Supply A exhibited a grain size of approximately ASTM 14 versus the previously determined size of ASTM 12 for supply B.[1] This difference in grain size helps to explain the increased yield strength of supply A. The size and shape of the pearlite colonies in supply A is also noteworthy. The colonies are very small (cannot be resolved at this magnification) and are widely dispersed. These observations will be referred to in subsequent discussions of fracture surface micromorphology.

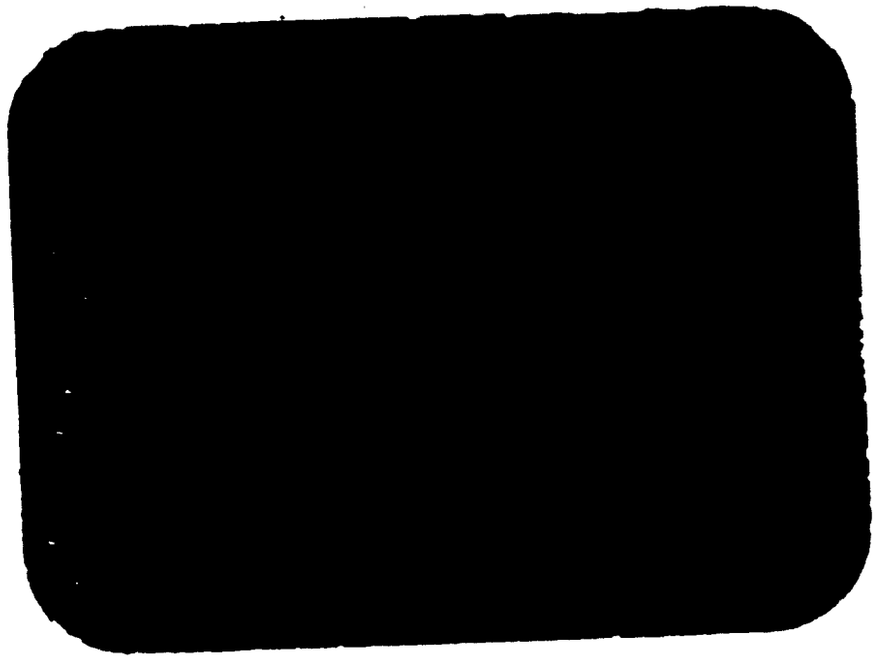

Fig. 5a Longitudinal section of VAN-80, Supply A
Magnification: 200X

Fig. 5b Transverse section of VAN-80, Supply A
Magnification: 200X

Fig. 6a Longitudinal section of VAN-80, Supply A
Magnification: 500X

Fig. 6b Transverse section of VAN-80, Supply A
Magnification: 500X

Fig. 7a Longitudinal section of VAN-80, Supply B
Magnification: 200X

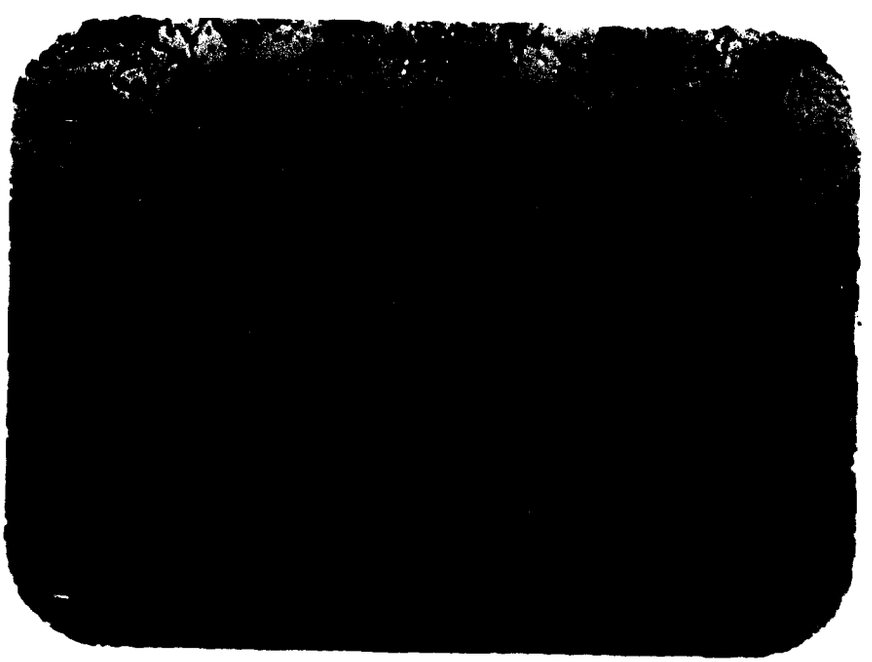

Fig. 7b Longitudinal section of VAN-80, Supply B
Magnification: 500X

High and low magnification photos of VAN-80 supply B (longitudinal to RD) are presented for comparison (Figures 7a and 7b). The larger grain size is readily apparent as in the increased size of the pearlite colonies (this pearlite is resolvable at 500X). By contrast, very little banding is observed in this material.

3.2 Crack Propagation Results and Discussion

Crack Growth Rate Test Results

Crack propagation test results are presented in Figures 8 and 9 as plots of crack growth rates ($\frac{da}{dn}$) vs. stress intensity range (ΔK). Least squares straight lines (log-log) have been fitted to this data according to the Paris power law relationship where

$$\frac{da}{dn} = C\Delta K^m \qquad (2)$$

Longitudinal specimens can be characterized by the equation $\frac{da}{dn} = 3.8 \times 10^{-9} (\Delta K)^{3.23}$ while propagation in transverse samples is characterized by the equation $\frac{da}{dn} = 5.3 \times 10^{-9} (\Delta K)^{3.14}$. For all practical considerations, these equations describe the same line for crack growth rates of interest in the range of 10^{-6} to 10^{-2} mm/cycle. The mechanical isotropy is, once again, evident in terms of crack propagation behavior. The lines described by these two expressions are presented in Figure 10 along with a line representing the equation $\frac{da}{dn} = 6.89 \times 10^{-9} (\Delta K)^3$. This latter equation describes growth rates in many normal ferrite-pearlite

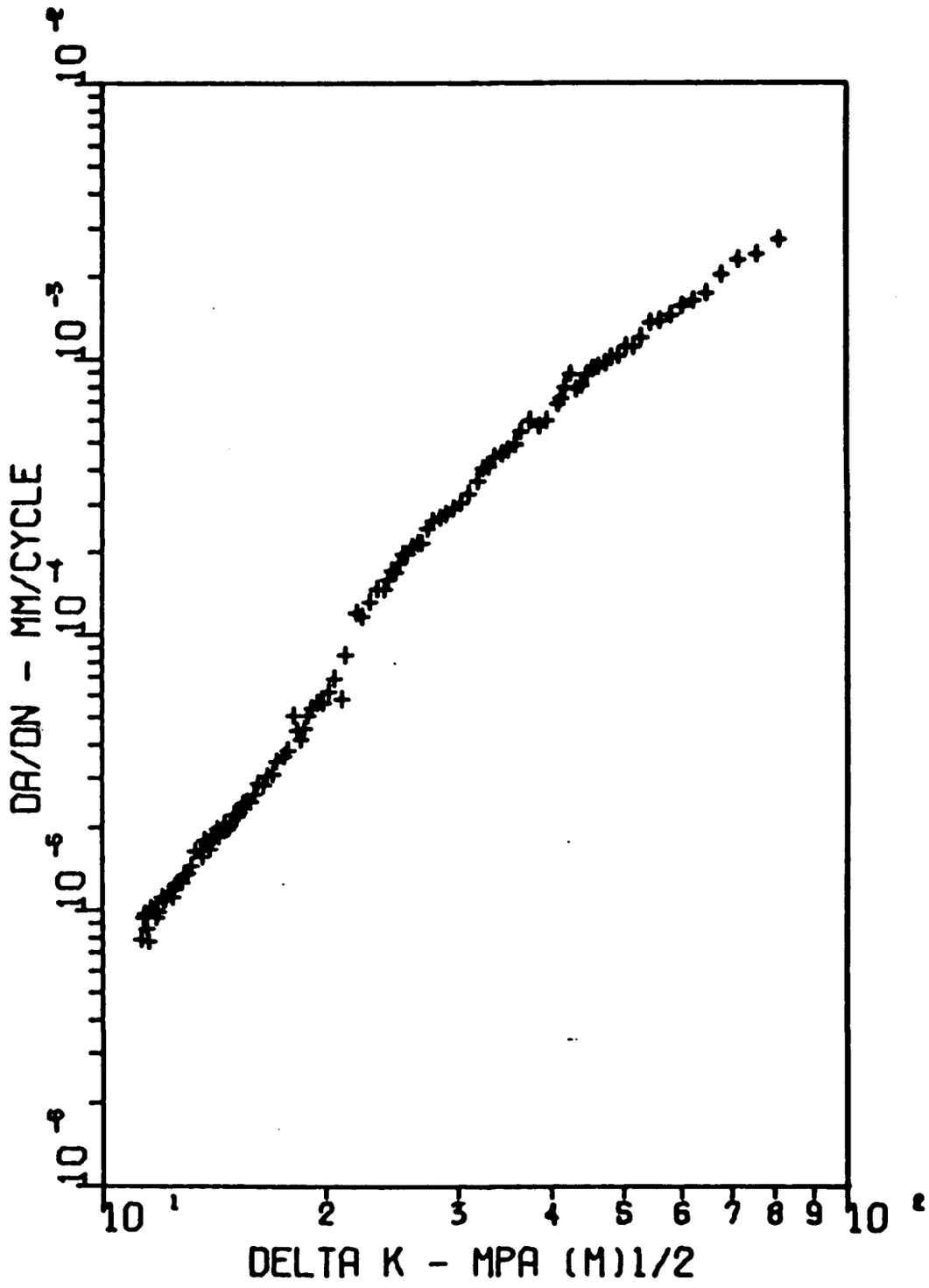

Figure 8 - da/dn VS. ΔK For VAN-80 Supply A Listed In The L-T Orientation

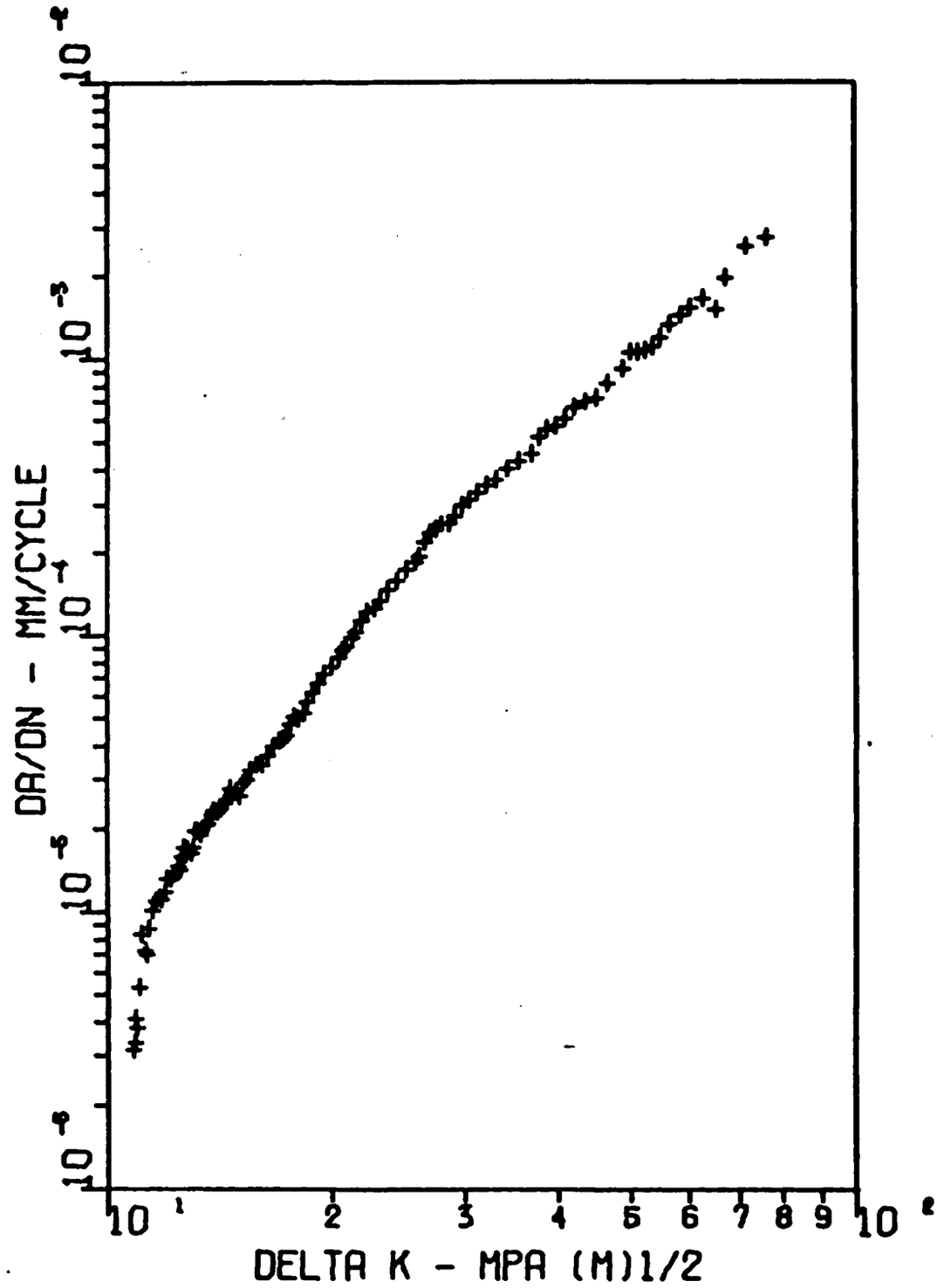

Figure 9 - da/dn VS. ΔK For VAN-80 Supply A Tested In The T-1 Orientation

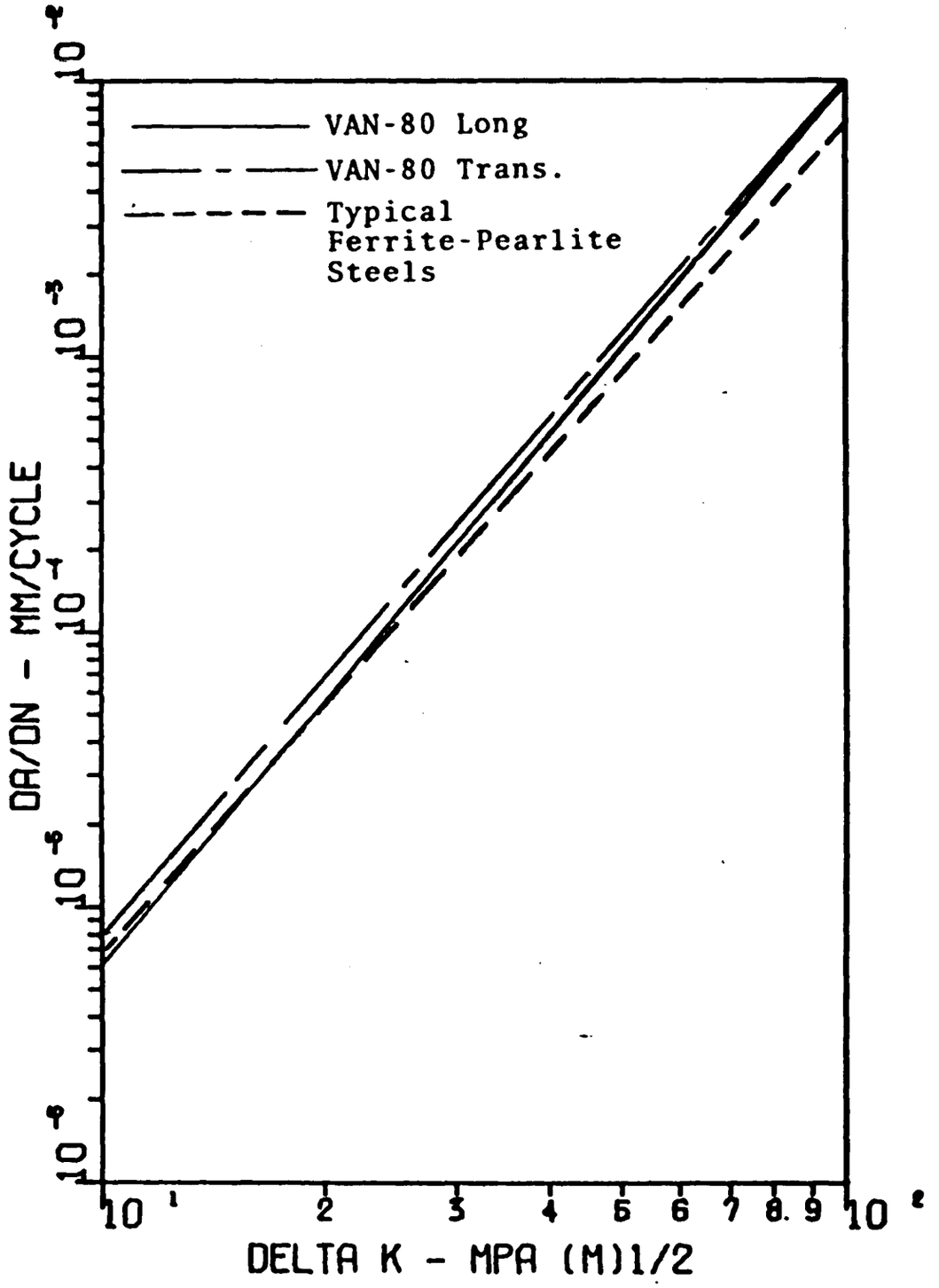

Figure 10 - Graph Showing Least Square Fit Lines Of da/dn VS. ΔK For T-L and L-T Orientations.

steels.[13] It can be seen that the fatigue crack growth behavior in VAN-80 compares well with this generalized expression; the FCP data are in agreement even though the yield strength of VAN-80 is significantly higher than that of the other ferrite-pearlite steels. Also, VAN-80 grain size is 8-16 times smaller than found in other ferrite-pearlite steels. In addition, little change in crack growth rates was noted between VAN-80 supply A and the previously tested supply B.

FRACTOGRAPHIC OBSERVATIONS

A complete characterization of fracture surface micromorphology at low growth rates was conducted on VAN-80 crack propagation specimens from supplies A and B.

VAN-80 Supply B

At intermediate stress intensity levels, striation formation was shown to be the primary crack growth mechanism.[1] The lowest stress intensity range for which striations were observed in this study was 16.8-17.6 MPa$\sqrt{m}$. This corresponded to a macroscopic growth rate of 1.27-1.46 X 10^{-5} mm/cycle. Striation spacing widths were measured and found to be in the range of 4.9-5.6 X 10^{-5} mm/cycle. The observed difference between macroscopic and microscopic growth rates at these low ΔK levels is not unusual as described previously.[14] However, the measured striation spacing is in good agreement with the prediction based on the Bates and Clark relationship[15]

$$\text{striation spacing} = 6\left(\frac{\Delta K}{E}\right)^2, \qquad (3)$$

which yielded values of 4.0-4.3 X 10^{-5} mm/striation.

At ΔK levels of 16.8-17.6 MPa$\sqrt{m}$, about 20% of the fracture surface exhibited pearlite boundary failure (PBF); i.e., the fracture path followed some boundaries of the pearlite colonies (Figure 11). At these stress intensity levels, there was limited evidence of through-pearlite failure and of faceting (i.e., transcrystalline failure along specific crystal planes) as reported for other materials.[12] Figure 12, however, shows faceting, pearlite boundary failure, and possible evidence of striations in the same vicinity.

Striations could no longer be seen at somewhat lower levels of ΔK (16-16.7 MPa$\sqrt{m}$). Here, pearlite boundary failure was at a maximum; approximately 50% of the fracture surface exhibited PBF. With a carbon content of 0.14%, VAN-80 should contain only 16% pearlite. For 50% of the fracture surface to show PBF, failure at these stress intensity levels must occur preferentially at pearlite-ferrite interfaces. Other investigators have previously noted such a preference for PBF in normal ferrite-pearlite steels.[7-11,13] In addition, the remainder of the fracture surface yielded many examples of intergranular failure along ferrite-ferrite boundaries.

Due to the existence of ferrite-ferrite intergranular failure, it was possible to measure grain size. The

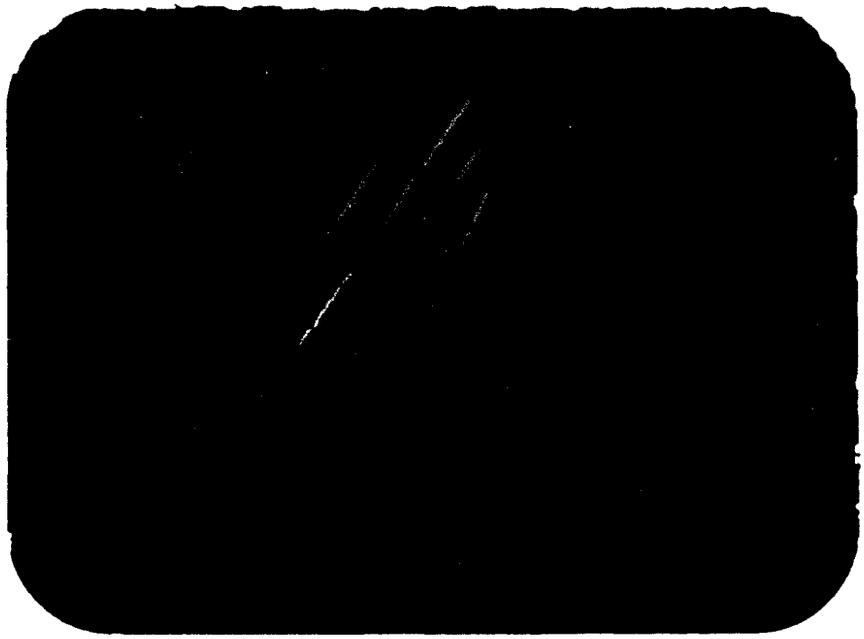

Fig. 11 Typical pearlite boundary failure as seen in VAN-80, Supply B. 21250X, TEM.

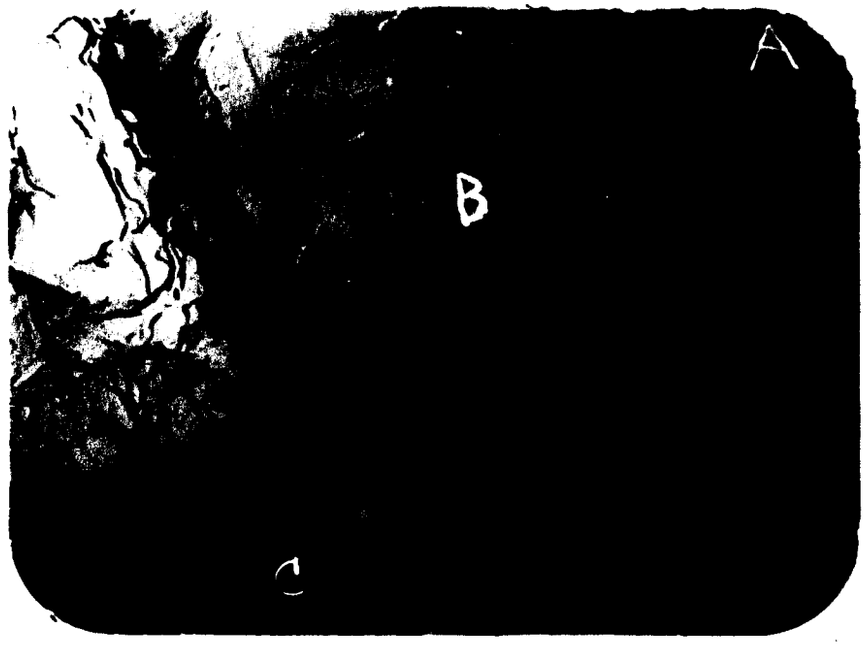

Fig. 12 Pearlite boundary failure (A), faceting (B), and possible striations (C) seen in VAN-80, Supply B. 21250X, TEM.

grain diameters were found to be approximately 3.6×10^{-3} mm. By comparison, the reversed plastic zone size for this stress intensity level, given by

$$r_y = \frac{1}{6\pi} (K/2\sigma_{ys})^2, \qquad (2)$$

was found to be 1.2×10^{-2} mm. Other researchers reported a 1:1 relationship between the reversed plastic zone size and the grain diameter at the point of a fracture mechanism transition from a structure sensitive fracture surface morphology (PBF and ferrite intergranular failure) to a structure insensitive fracture surface morphology (fatigue striations).[7-9,11] The difference between the 1:1 ratio and the present experimentally determined 3:1 ratio is not clearly understood but may be due in part to the extremely small grain size of the VAN-80 steel.

Pearlite boundary failure persisted at lower ΔK levels (15.4-16 MPa$\sqrt{m}$), though to a lesser extent. At this stress intensity level, pearlite lamellae failure in conjunction with PBF was also observed (Figure 13). At the same time, the amount of ferrite-ferrite intergranular failure increased to such an extent that this became the primary fracture mode. In addition, there again was limited evidence of faceting.

The lowest ΔK levels available for observation in VAN-80 supply B were 13.4-13.7 MPa$\sqrt{m}$. Very little PBF was observed. Very little faceting and little ferrite-ferrite intergranular failure were seen. Thus, the

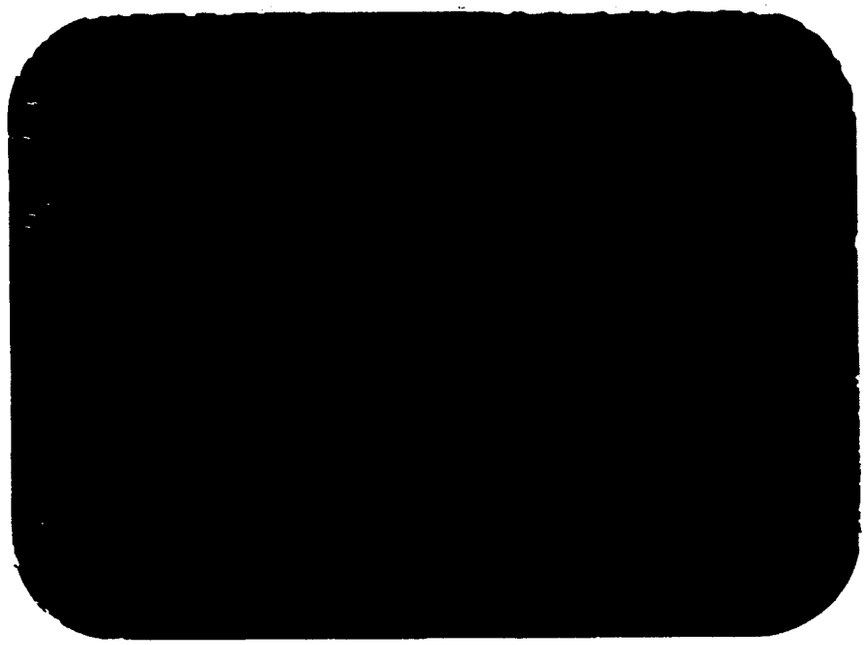

Fig. 13 Pearlite boundary failure and pearlite lamellae failure seen in VAN-80, Supply B. 16250X, TEM.

Fig. 14 Typical striations seen in VAN-80, Supply A at a stress intensity range of 22-23 MPa$\sqrt{m}$. 45000X,TEM.

fracture surface was generally featureless. These stress intensity levels produced the smallest reversed plastic zone available for study (r_y=8 X 10^{-3}mm, still two to three times larger than the grain diameter). Consequently, the present fractographic observations tend to dispute the previously reported observation that a 1:1 ratio of grain size to plastic zone size signalled a transition from structure sensitive to structure insensitive crack growth.

VAN-80 Supply A

The highest ΔK level examined in this part of the study was 32-35 MPa$\sqrt{m}$. The vast majority of the fracture surface in this region was striated, as expected. Macroscopic growth rates are compared in Table III with striation spacing and predicted striation spacing for all stress intensity levels which yielded striations. At a ΔK level of 22-23 MPa$\sqrt{m}$, the fracture surface was still fully striated.

Decreasing the stress intensity range to 17 MPa$\sqrt{m}$ caused a change in fracture surface appearance. Approximately 50% of the surface was still striated. In addition, pearlite boundary failure and ferrite-ferrite intergranular failure were observed, each accounting for 10% of the total fracture surface. Thus, the transition had begun from structure insensitive to structure sensitive crack growth. The ratio of reversed plastic zone

TABLE III: MACROSCOPIC GROWTH RATES, STRIATION SPACING, AND PREDICTED STRIATION SPACING

ΔK MPa$\sqrt{m}$	Macro Growth Rate mm/Cycle	Striation Spacing mm/Striation	Bates & Clark Prediction mm/Striation
32-35	4×10^{-4}	1.2×10^{-4}	1.6×10^{-4}
22-23	1.4×10^{-4}	5.9×10^{-5}	7.7×10^{-5}
17	3.6×10^{-5}	3.7×10^{-5}	4×10^{-5}
16	2.9×10^{-5}	2.8×10^{-5}	3.6×10^{-5}
14	2×10^{-5}	2.8×10^{-5}	3×10^{-5}

size to grain diameter was approximately 6:1 at this point.

When ΔK decreased to 16 MPa$\sqrt{m}$, 40% of the surface was still striated. Approximately 20% of the surface exhibited PBF while another 20% showed ferrite-ferrite intergranular failure. Figure 15 shows PBF typical of supply A. This colony can be characterized as a degenerate form of pearlite with globular rather than lamellar carbides. This small, degenerate colony is in marked contrast to the large, well-formed pearlite colonies found in supply B (Figure 11).

Upon further reduction of ΔK to 14 MPa$\sqrt{m}$, very few striations were observed. Ten to fifteen percent of the fracture surface exhibited PBF while ferrite-ferrite intergranular failure accounted for 70% of the fracture surface. At ΔK levels of 11-13 MPa$\sqrt{m}$, striations were no longer present. PBF in this region never exceeded 25% of the fracture surface. At a ΔK level of 11 MPa$\sqrt{m}$, a small decrease in the total amount of intergranular failure was noticed. This was the lowest stress intensity level available for study; with intergranular failure once again on the decline, it should be noted that the ratio of reversed plastic zone size to grain size was still greater than 2:1. Thus, the 1:1 ratio proposed by other authors for the fracture mechanism transition does not adequately describe the behavior of VAN-80.

Fig. 15 Degenerate pearlite boundary failure as observed in VAN-80, Supply A. 56250X, TEM.

It is apparent that material supply A, while showing the same total amounts of intergranular failure, shows much less PBF than does supply B. The explanation may lie in the fact that the pearlite colonies are very small in supply A (very much smaller than the ferrite grains). By contrast, pearlite colonies in supply B are approximately the same size as the ferrite grains. Thus, in supply A, the pearlite colonies have very little surface area to present to the advancing crack; the crack could propagate only a very short distance before being forced to find another path. Ferrite-ferrite failure may then be preferred since once a ferrite grain boundary is reached, a relatively large advance along the grain is possible.

In summary, one of the more important results of this fractographic study was to extend the range over which fractographic observations can be used to infer the magnitude of a prevailing stress intensity level. The presence of intergranular failure alone thus indicated a stress intensity range of 10-14 MPa$\sqrt{m}$ in the VAN-80 alloy.

3.3 Crack Initiation Results and Discussion

Base Line Crack Initiation

Results of studies concerning crack initiation at three finite radii notches (ρ = 0.79, 1.59, and 3.18 mm, respectively) are presented in Figure 16 as plots of applied stress intensity range (ΔK) versus crack initiation

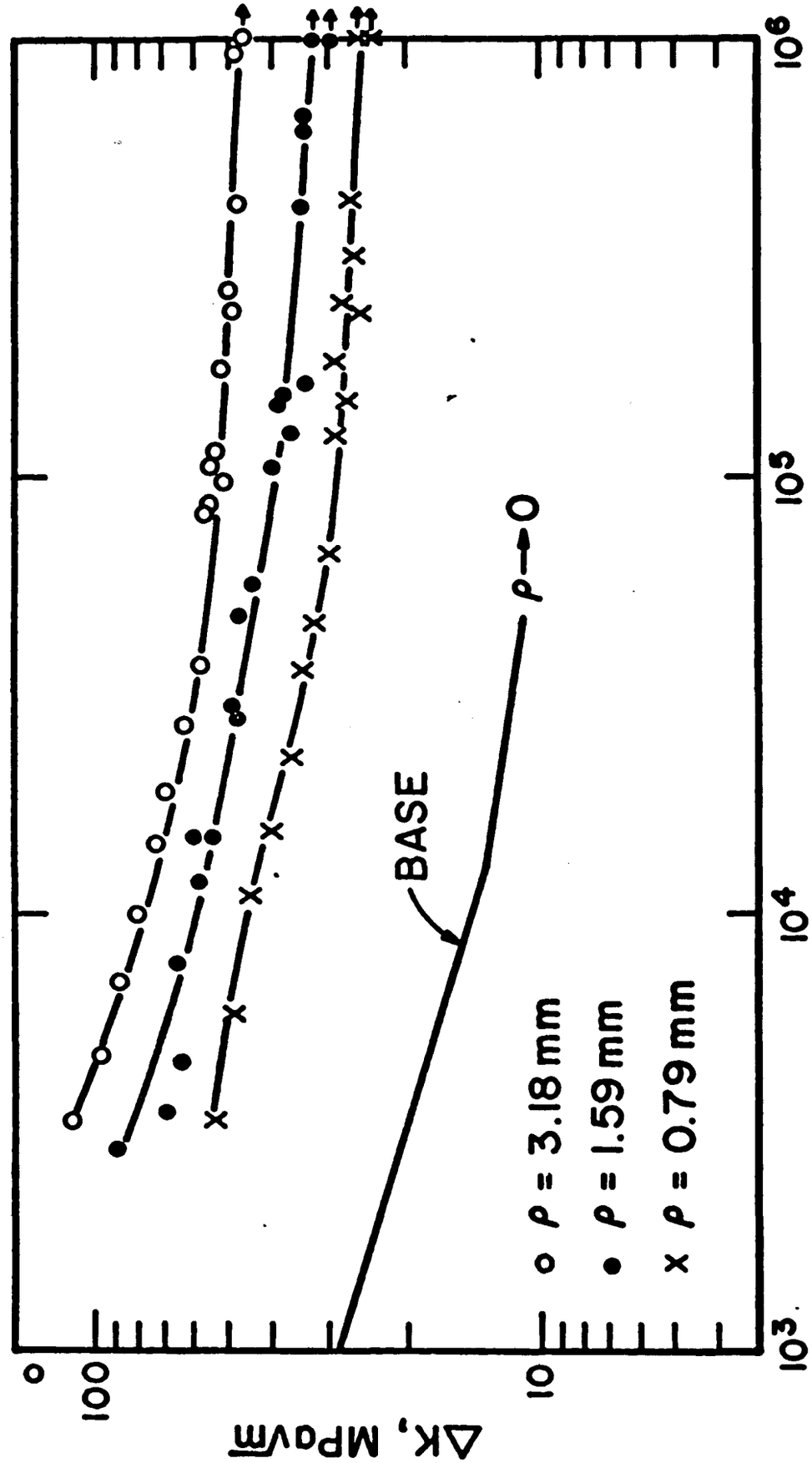

Fig. 16 ΔK VS. N_I, composite of all base-line data.

life (N_I). The definition of crack initiation used here combines both the actual initiation of a crack and subsequent propagation to a length of 0.25 mm. Therefore, the condition of $\rho \rightarrow o$ i.e., a sharp crack, was also considered; N_I for this case was determined strictly from previously obtained crack propagation data. As expected, a distinct separation of the results obtained from each notch radius was observed. The sharper the notch and the greater the associated stress concentration factor, the lower the applied ΔK needed for crack initiation at any given number of cycles.

Maximum cyclic stress at the notch root is given by[3]

$$\Delta \sigma = \frac{2\Delta K}{\sqrt{\pi \rho}} \qquad (4)$$

As shown by others[2-4], the parameter $\frac{\Delta K}{\sqrt{\rho}}$, which is directly proportional to $\Delta \sigma$, may be used to normalize crack initiation data from notches of varying radii. This normalization of the current data is presented in Figure 17. Since $\rho \rightarrow o$ for the sharp crack, no normalization of this data is possible.

This normalization by the use of $\frac{\Delta K}{\sqrt{\rho}}$ also allows one to speak of a threshold $\frac{\Delta K}{\sqrt{\rho}})_{TH}$. Cycling at or below this value would preclude crack initiation[3]. This would then be analogous to the fatigue limit in traditional "S-N" tests. During the investigation, VAN-80 was found to exhibit a $\frac{\Delta K}{\sqrt{\rho}})_{TH}$ of 835 MPa at 10^6 cycles. Other widely used steels have yielded values of $\frac{\Delta K}{\sqrt{\rho}})_{TH}$

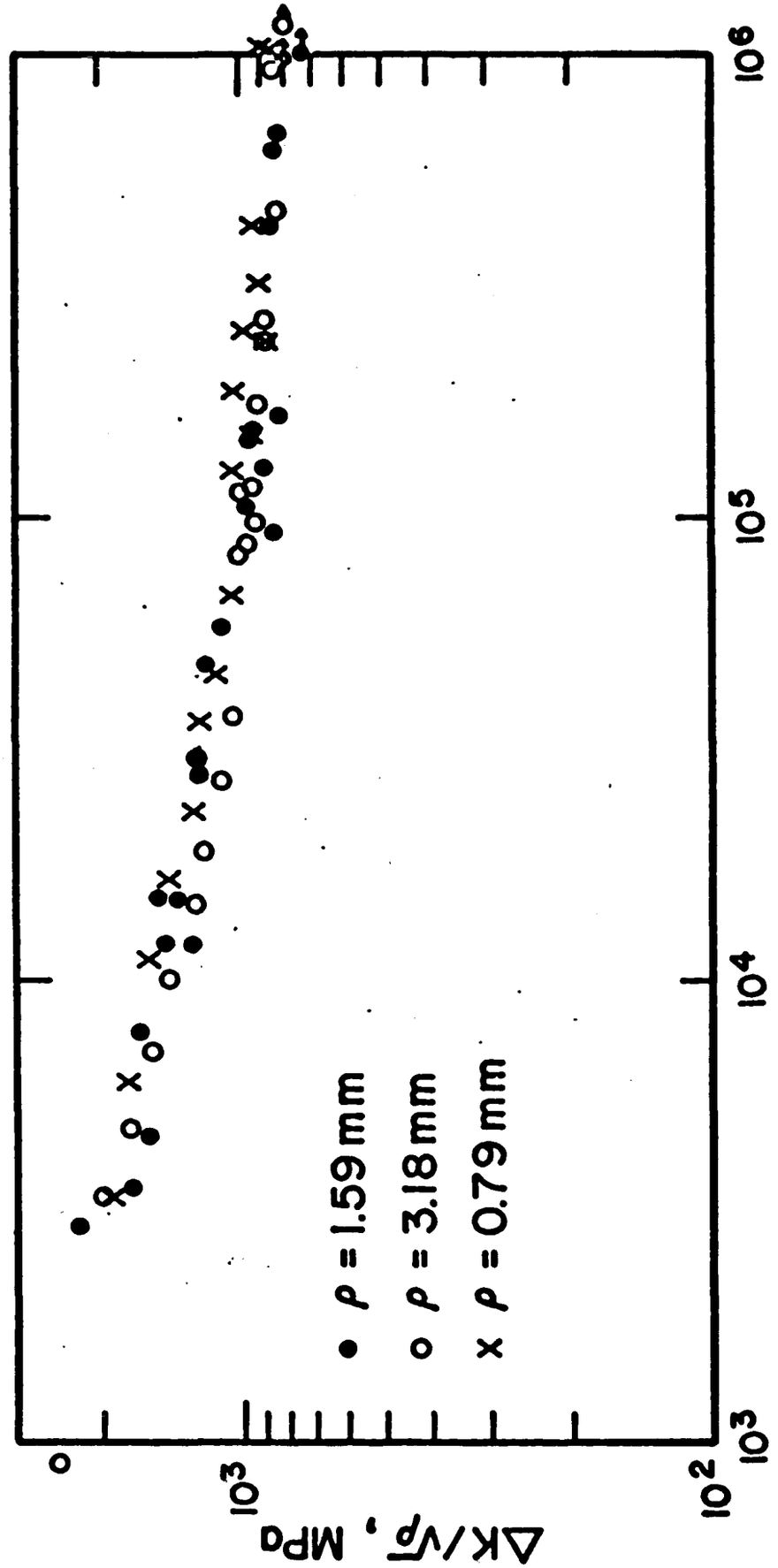

Fig. 17 $\Delta K/\sqrt{\rho}$ VS. N_I, composite of all base-line data.

which ranged from 420 MPa to 900 MPa.[3,4,14] Various correlations have been attempted between $\frac{\Delta K}{\sqrt{\rho}})_{TH}$ and tensile strength, yield strength, or strain hardening exponent. Unfortunately the value of $\frac{\Delta K}{\sqrt{\rho}})_{TH}$ cannot be predicted by use of these correlations.

It is apparent from figure 17 that use of the parameter $\frac{\Delta K}{\sqrt{\rho}}$ does not result in a total normalization of the data. For a given life, a lower value of $\frac{\Delta K}{\sqrt{\rho}}$ is needed to initiate a crack as ρ increases. This again confirms the volume effect as described by others [3,4] and is most easily described by referring to Figure 18. While $\frac{\Delta K_1}{\sqrt{\rho_1}} = \frac{\Delta K_2}{\sqrt{\rho_2}}$, it can be seen that the stress gradient is much larger for the case involving the small notch radius. Therefore, the smaller the radius, the smaller will be the volume of material ahead of the notch root that is subjected to stresses above some critical level. With less material subject to stresses, there is a correspondingly smaller probability of finding a suitable site for easy crack initiation.

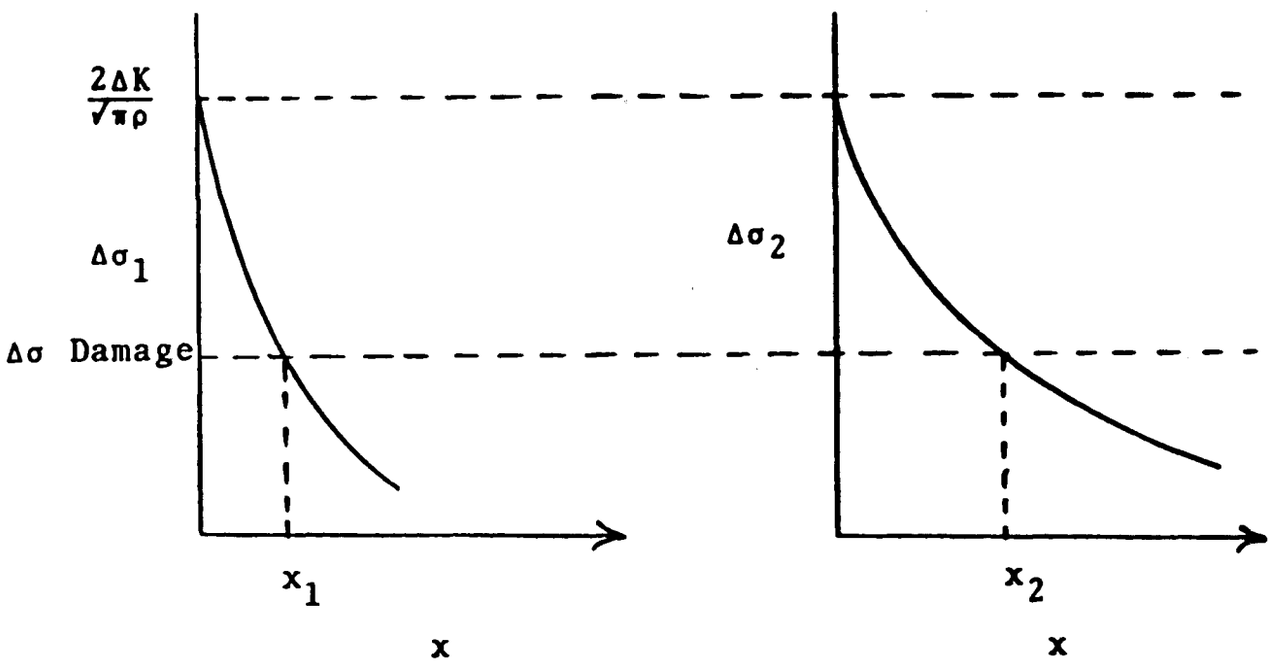

$$\frac{\Delta K_1}{\sqrt{\rho_1}} = \frac{\Delta K_2}{\sqrt{\rho_2}}$$

$$\rho_2 > \rho_1$$

x = Distance from notch root

Figure 18 - Volume Effect

High Block-Low Block Initiation Results

Until now, it has been tacitly assumed that there is indeed such a thing as crack initiation. Everyone does not take this position; there are those who contend that the fatigue process consists only of crack propagation.

Miner's Law For Cumulative Damage

Miner's Law[16] is the simplest cumulative damage model presently in use. Miner's law assumes no interaction between different block loads and no sensitivity to load sequence. According to this theory, if N cycles are necessary for fatigue failure at a given stress level, it is assumed that $\frac{n}{N}$ fraction of the entire life of the sample is consumed when a component experiences n cycles at that same stress level. It follows that when a series of block loads is applied to the sample, failure is assumed to occur when $\Sigma\frac{n}{N} = 1$. If this relationship held true in all cases, it would greatly simplify our understanding and analysis of the fatigue process. Unfortunately, this is not found to be the case.

At times $\Sigma\frac{n}{N}$ is found to be greater than one and in other tests, this summation is less than one. It has been shown that notch acuity exerts a strong influence on crack initiation life under block loading conditions. Kommers found that under high block-low block loading conditions in unnotched specimens, $\Sigma(\frac{n}{N})$ was less than one. This would indicate that the initial high load block caused more damage than predicted by Miner's law. Crack nucleation is believed to be hastened by the high block; the following low load block involves only propagation of this nucleated crack. Contrasted with this is the fact that Hudson

and Hardrath [17] and Schijve and Broek [18] have shown that $\Sigma(\frac{n}{N})>1$ for the case of specimens containing sharp notches. The explanation for this opposite effect may be traced to crack growth rate retardation resulting from the presence of favorable residual stress and/or crack closure effects as reported by several authors for various materials.[19,20,21]

Thus, if a sample containing a notch of known severity is subjected to high block-low block loading conditions, the relative importance of crack initiation versus crack propagation may be determined. That is, if such tests show $\Sigma(\frac{n}{N})<1$, then one would conclude that the fatigue process is dominated by true initiation; however, if $\Sigma\frac{n}{N}>1$, then the propagation stage would appear to dominate the overall process.[22]

Results of high block-low block tests on two finite radii notches (ρ= 1.59 and 3.18 mm) are presented in Figures 19 and 20. These figures also contain the base-line initiation data and curves which represent Miner's Law expectations ($\Sigma\frac{n}{N}=1$) for the high block-low block tests. Test results from a sharp crack ($\rho \rightarrow o$) are presented in Figure 21. This case gives the reader an indication of the susceptibility of VAN-80 to overload induced crack delay effects. Again, base-line date and Miner's law expectations are provided for comparison.

It is apparent that for all high block-low block

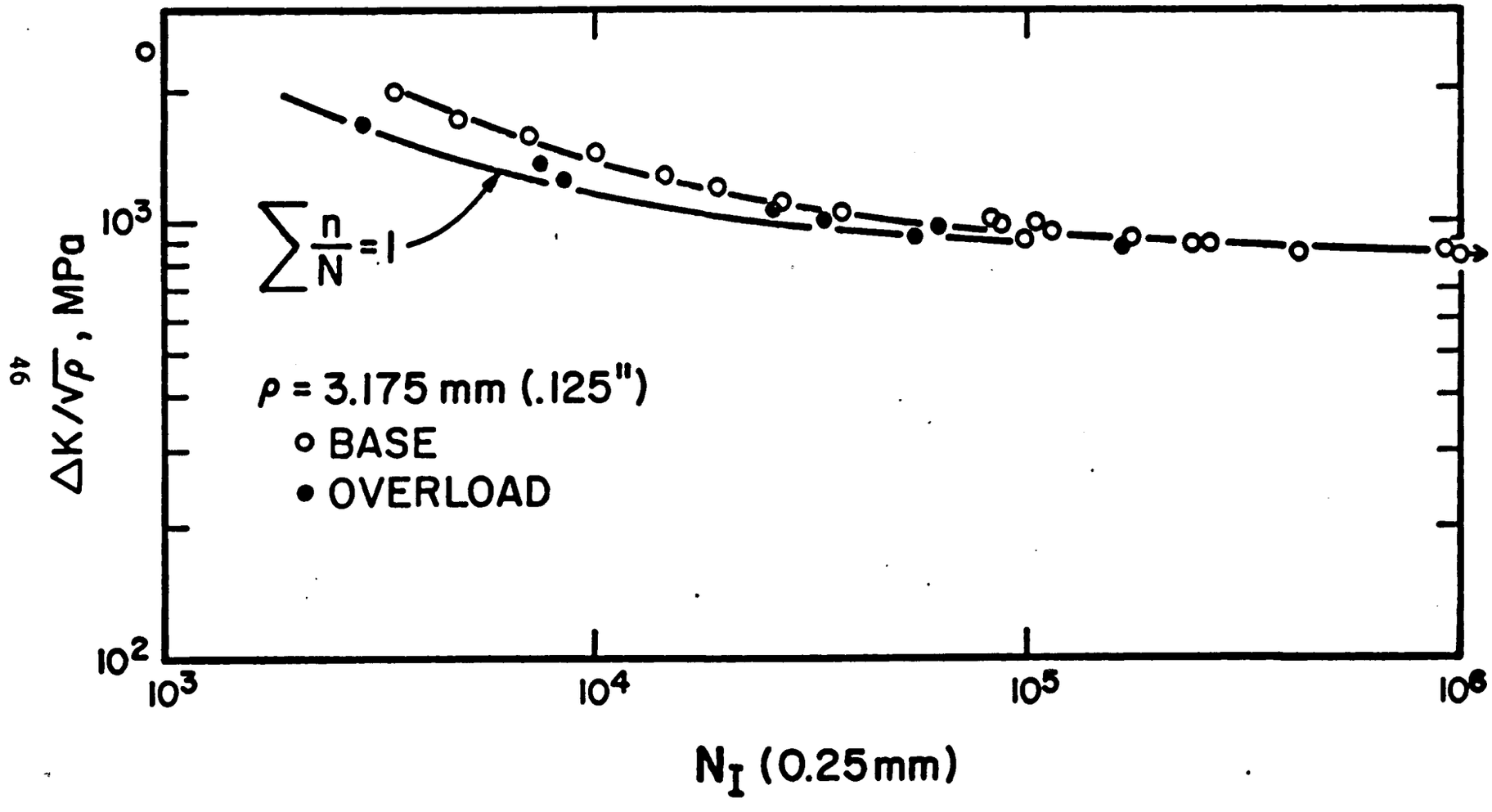

Fig. 19 $\frac{\Delta K}{\sqrt{\rho}}$ VS. N_I for ρ = 3.18 mm, including base-line and block load results.

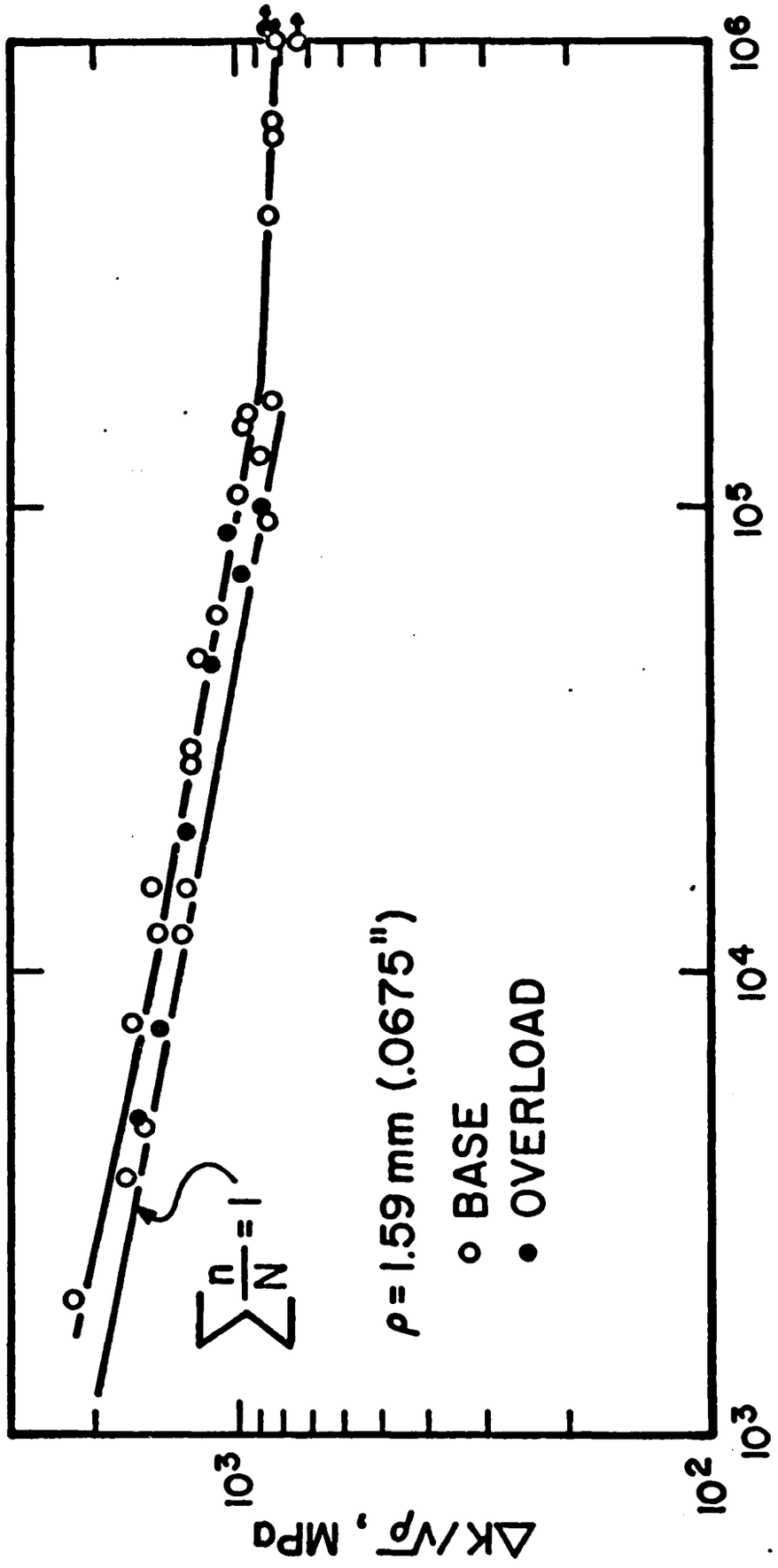

Fig. 20 $\frac{\Delta K}{\sqrt{\rho}}$ VS. N_I for ρ = 1.59 mm, including base-line and block load results.

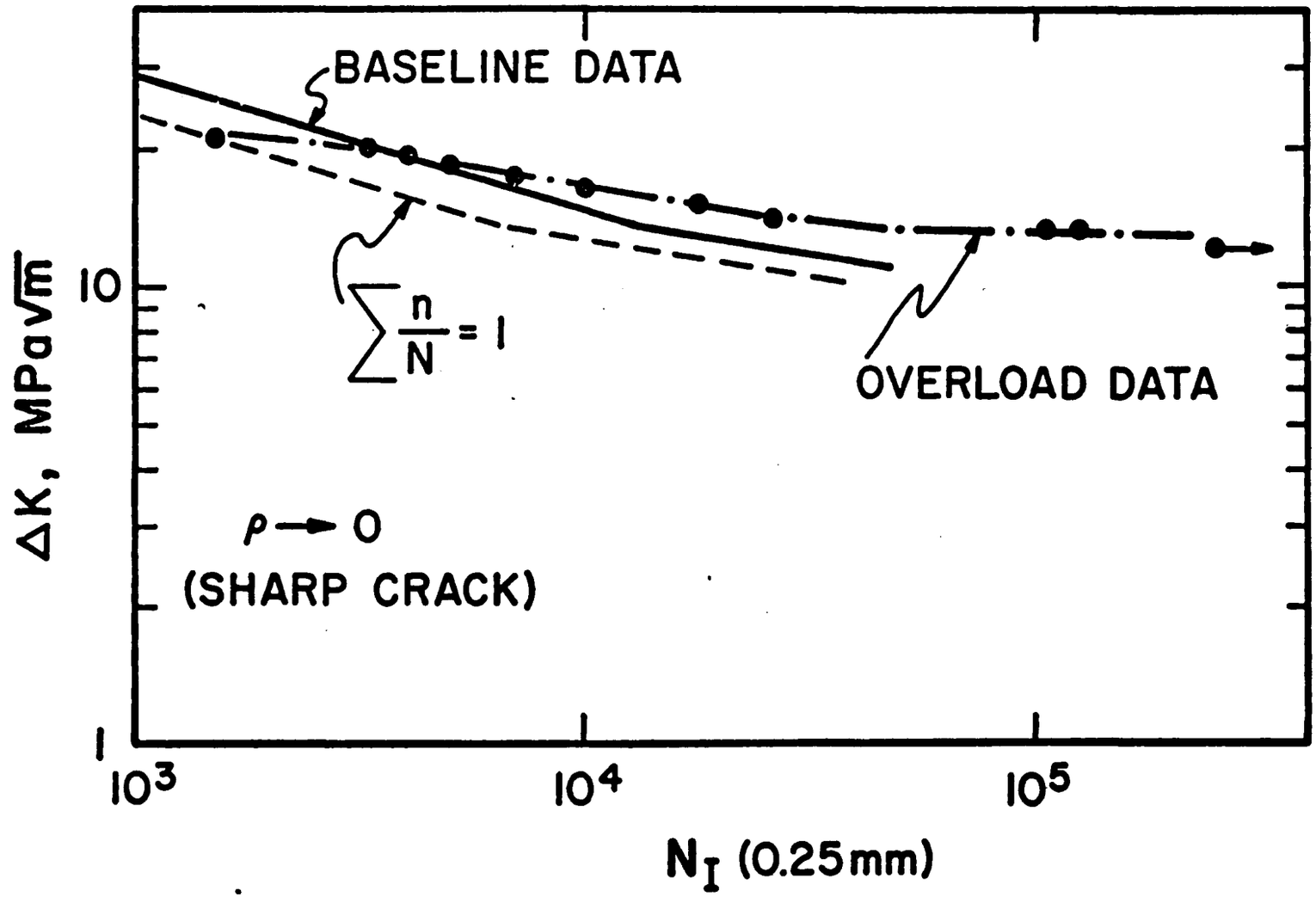

Fig. 21 ΔK VS. N_I for $\rho \rightarrow o$ (sharp crack), including baseline and block load results.

tests, $\Sigma\frac{n}{N}>1$. By the reasoning presented earlier, it would appear that for all notch radii examined, crack propagation dominated the fatigue process. Additional comments pertaining to this conclusion are given in the next section with respect to certain fractographic observations.

Particular attention at this time should be given to Figure 21 which reflects the susceptability of VAN-80 to overload induced crack retardation. Not only is $\Sigma(\frac{n}{N})>1$ for all test conditions, but under any overload more than 8% greater than the low block load, $\Sigma(\frac{n}{N})>1.5$; i.e., the data will fall to the right of the base-line curve. When the high block was 70% higher than the low block, complete crack arrest occurred with no growth whatsoever observed after a quarter million cycles. VAN-80 is therefore seen to be extremely sensitive to overload induced growth rate retardation.

With this severe retardation potential in mind, a modified explanation of the high block-low block finite radius results is deemed appropriate. To begin, it is restated that the arbitrarily chosen criterion for crack initiation involves 0.25 mm of crack propagation. Consequently, it may be argued that retardation within this 0.25 mm increment of crack growth, due to compressive residual stresses and/or closure which was induced by the high load block, may overshadow the actual damage

caused by the high block. That is, the high block may still hasten initiation; however, the resultant small crack at the notch root will grow extremely slowly and consume many cycles before fulfilling our definition of initiation. For example, crack growth rates within the high block affected zone were decreased by 1 to 1.5 orders of magnitude. A revised definition of crack initiation is, therefore, needed if one would wish to separate initiation and propagation stages of the fatigue process. A new definition of initiation would only be advantageous if available crack detection methods could accurately detect smaller cracks.

FRACTURE SURFACE OBSERVATIONS

Selected specimens obtained during base-line crack initiation testing and during high block-low block testing were subjected to macroscopic and microscopic (TEM & SEM) fracture surface examination.

Macroscopic Examination

Macroscopic fracture surface examination immediately revealed one very important point common to both base-line test specimens and high block-low block samples. At relatively low test values of $\frac{\Delta K}{\sqrt{\rho}}$ MPa (less than 1000 MPa) single initiation sites were observed (Figures 22a & b, arrow A). By contrast at relatively high values of $\frac{\Delta K}{\sqrt{\rho}}$ (> 1000 MPa), multiple crack initiation sites were observed (Figures 23 a & b, arrow A). This may be

Fig.22a Macrophoto of typical base-line specimen cycled under low $\frac{\Delta K}{\sqrt{\rho}}$ conditions revealing a single origin. 17X

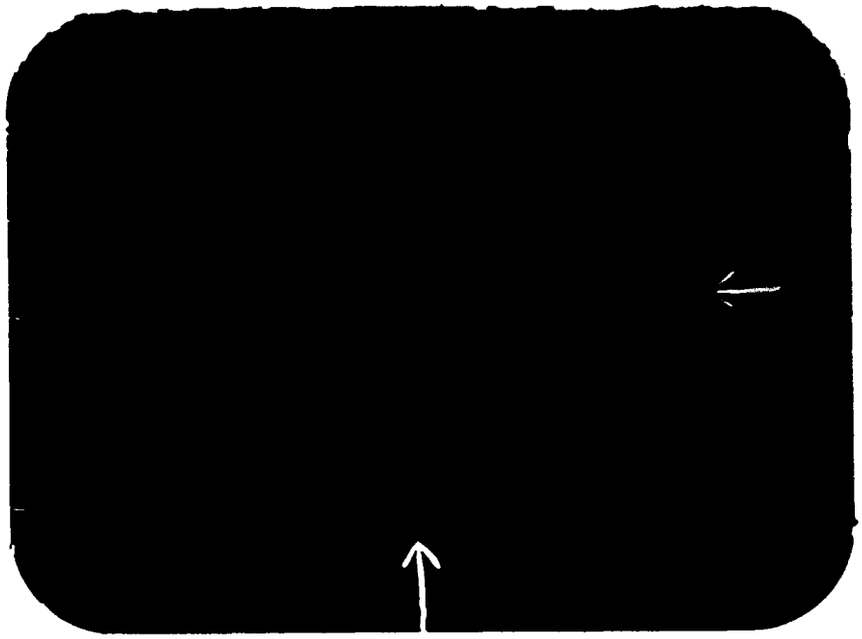

Fig.22b Macrophoto of typical high block-low block specimen cycled with low $\frac{\Delta K}{\sqrt{\rho}}$ value for the "low block". A single crack origin is noted. (A)

Fig. 23a Typical base-line specimen cycled at high $\frac{\Delta K}{\sqrt{\rho}}$ levels, exhibiting multiple origins. 17X

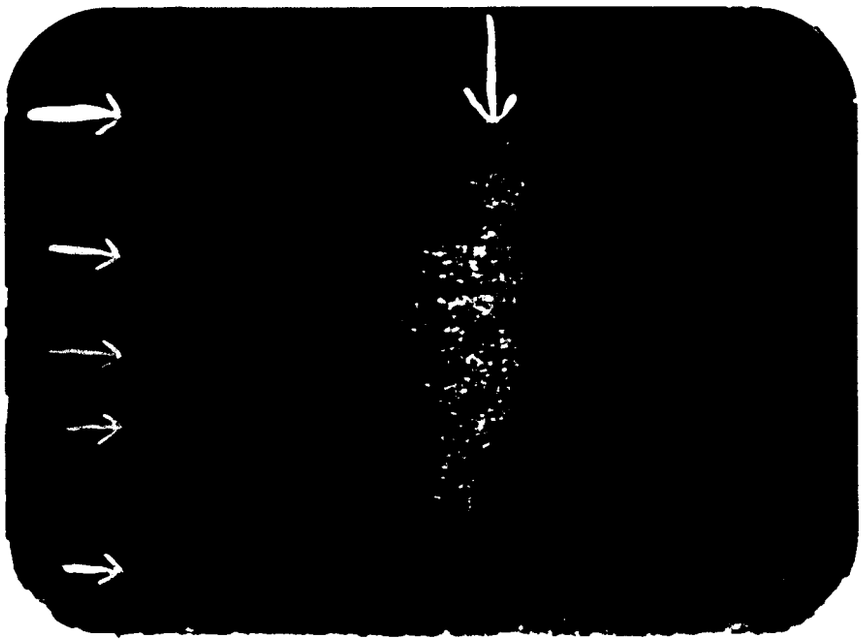

Fig. 23b Typical high block-low block specimen cycled at high $\frac{\Delta K}{\sqrt{\rho}}$ during the low block exhibiting multiple origins. 17X

attributed to the fact that at high stress levels, there are more potential crack initiation sites. The fact that this same phenomena was not observed in the high block-low block is significant. This indicates that very small cracks were not present at the end of the high block sequence. If small cracks had been present, some growth would be expected during the low block and multiple origins would be easily visible. Thus, it is concluded that crack initiation took place during the low load block.

Another macroscopic observation common to both testing conditions concerns the location of initiation sites on the fracture surface. The vast majority of cracks initiated at the polished surface away from the corners of the sample. Very few corner cracks were observed, even though the local stress level is presumed to be higher at the corners. Other investigations [23] have shown the same results in regard to initiation site location.

The final macroscopic observations pertain to the block loaded specimens. Visible evidence of plastic deformation at the notch root (necking) occurred during the high block loading sequence. The fracture surfaces within this plastic zone were covered with a light brown oxide; a clear delineation on the fracture surfaces was visible at the end of this plastic zone

(refer to Figures 22b & 23b, arrow B). Since specimens were stored in a dessicator immediately after testing, it is doubtful that this oxide was the result of normal atmospheric corrosion (rusting). Outside the plastic zone, no corrosion products were found although the entire sample was subjected to the same environment at all times.

It is worthwhile to compare the size of this visually determined damage zone with the calculated size of the plastic zone. This was done using Creager's analysis for the elastic stress state distribution around a blunt notch.[24] Accordingly

$$\sigma_x = \frac{K}{\sqrt{2\pi r}} \cos\frac{\theta}{2} \left(1 - \sin\frac{\theta}{2} \sin\frac{3\theta}{2}\right) - \frac{K}{\sqrt{2\pi r}} \frac{\rho}{2r} \cos\frac{3\theta}{2} \quad (5)$$

$$\sigma_y = \frac{K}{\sqrt{2\pi r}} \cos\frac{\theta}{2} \left(1 + \sin\frac{\theta}{2} \sin\frac{3\theta}{2}\right) + \frac{K}{\sqrt{2\pi r}} \frac{\rho}{2r} \cos\frac{3\theta}{2} \quad (6)$$

$$\tau_{xy} = \frac{K}{\sqrt{2\pi r}} \sin\frac{\theta}{2} \cos\frac{\theta}{2} \cos\frac{3\theta}{2} - \frac{K}{\sqrt{2\pi r}} \frac{\rho}{2r} \sin\frac{3\theta}{2} \quad (7)$$

Where K = stress intensity level

ρ = notch radius

r = distance from notch root plus the distance $\frac{\rho}{2}$

Using the maximum octahedral shear stress criterion for yielding and knowing the material yield strength, the extent of the plastic zone can be determined through the use of a simple computer program. For example, a calculated plastic zone size of 3.9 mm was obtained for ρ=3.18 mm. Measurements of the damage zone extent from Figures 22b and 23b gave a value of 2.8 mm, which is in reasonably good agreement with the computed value.

TEM Examination

Base-line crack initiation samples were selected for a TEM fractographic study for the purpose of relating crack initiation site fracture surface micromorphology to known fracture surface micromorphology obtained during crack propagation tests. Transmission electron microscopy presents the investigator with several inherent difficulties which partially offset the desirable feature of excellent resolution. Obtaining a replica of an initiation site is no easy task; the site is invariably located at a sharp edge. If the initiation site is actually replicated successfully, replica edges curl, tear, and fold when placed on a grid. However, it is possible to examine areas of the fracture surface close to the origin and to characterize their appearance.

Many of the samples replicated during this stage of the investigation exhibited the entire range of fracture surface appearances. From striation spacing

data and the lack or presence of intergranular failure, local stress intensity levels could be estimated. Figure 24 shows large striations produced on a sample by an applied ΔK level of 68 MPa$\sqrt{m}$. The striation spacing is such that the implied ΔK level in this region is found to be only 22 MPa$\sqrt{m}$. Closer to the origin on the same replica, striation spacings decreased; the estimated ΔK level corresponding to these striations was 14-17 MPa$\sqrt{m}$.

Further evidence that the local stress intensity was considerably less than the remotely applied stress intensity was also observed. One specimen contained a 3.18 mm notch and was cycled at an applied $\Delta K/\sqrt{\rho}$ of 850 MPa (ΔK = 48 MPa$\sqrt{m}$, N_I = 935000). On the replica of interest, the furthest point from the origin was fully striated. The implied ΔK in this region was 30-32 MPa$\sqrt{m}$. Moving toward the origin, the fracture surface was still fully striated, but with an estimated ΔK level of 22 MPa$\sqrt{m}$ (Figure 25). Intergranular failure was first observed at an implied ΔK of 21 MPa$\sqrt{m}$. At an implied ΔK of 18 MPa$\sqrt{m}$, only 50% of the fracture surface exhibited striations. Intergranular failure was well defined and PBF was observed. At the edge of the replica (as close to the origin as possible), striations still accounted for 50% of the fracture surface. These striations yielded an implied ΔK of 15 MPa$\sqrt{m}$.

Fig. 24 Striations found in vicinity of origins; spacing is 1.05×10^{-4} mm/striation. Applied ΔK is 68 MPa$\sqrt{m}$. 25200X. TEM.

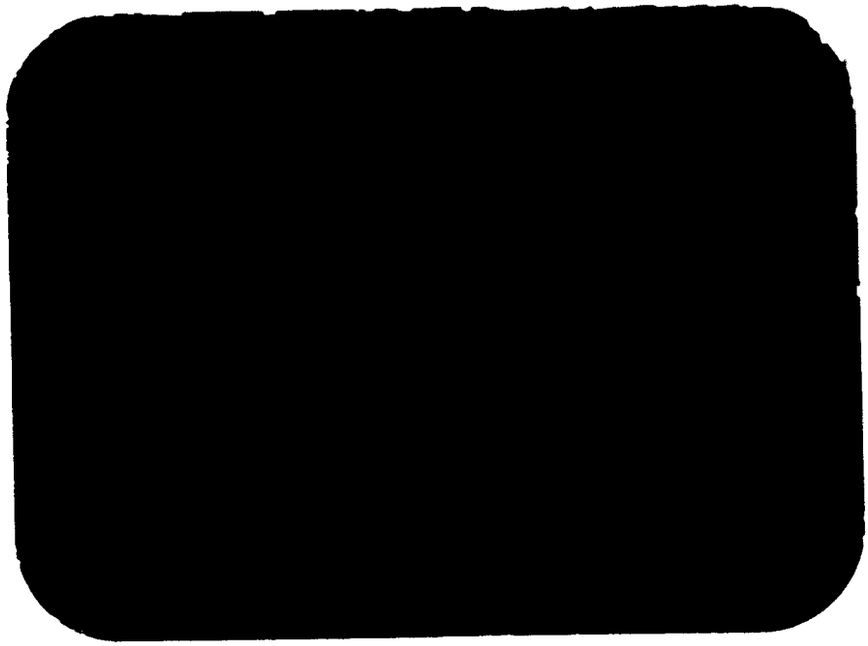

Fig. 25 Striations found in vicinity of origin with a striation spacing of 1.2×10^{-4} mm/striation. Applied ΔK is 48 MPa$\sqrt{m}$. 32640X, TEM.

Similarly, a second specimen exhibited this complete range of fracture surface micromorphology. This particular sample contained a 1.59 mm notch and was cycled at $\frac{\Delta K}{\sqrt{\rho}}$ = 850 MPa (ΔK = 34 MPa$\sqrt{m}$, N_I = 414,000). The largest striations found on the replica of interest implied a local ΔK of 21.5 MPa$\sqrt{m}$ (Figure 26); at this point approximately 75% of the surface was striated. At an implied ΔK of 18 MPa$\sqrt{m}$, intergranular failure began to increase; the transition from structure insensitive to structure sensitive crack growth began. Proceeding further toward the origin revealed an approximate 50-50 mixture of striations and intergranular failure (Figure 27). Still closer to the origin, striations disappeared while ferrite-ferrite boundary failure and PBF covered the fracture surface (Figure 28); from this overall appearance, one can imply a local ΔK level of 12-14 MPa$\sqrt{m}$ in this region. Based on fractographic results discussed earlier, it should be noted, however, that the applied ΔK level based on the blunt notch analysis was 34 MPa$\sqrt{m}$. At the edge of the replica, the fracture surface lost its intergranular character and became totally non-descript.

Based on these fractographic results, it is concluded that the local effective ΔK level for very short cracks in a notched compact tension specimen is much less than one would expect from the standard CT stress

Fig.26 Large striations on sample A2-54. Spacing is 1×10^{-4} mm/striation at an applied ΔK of 34 MPa$\sqrt{m}$. 25200X, TEM.

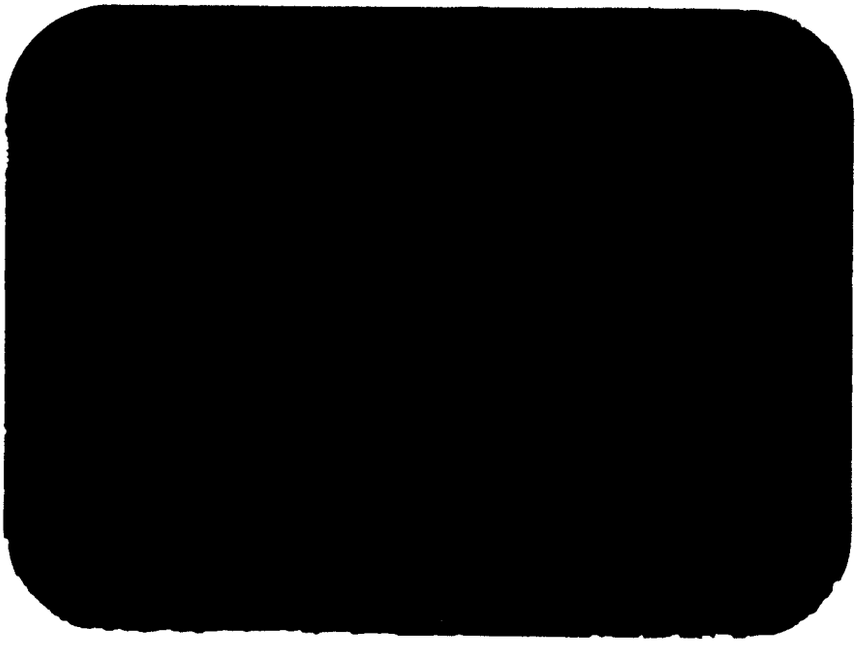

Fig.27 Small striations and pearlite boundary failure from sample A2-54. Striation spacing is 5.2×10^{-5}mm/striation at an applied ΔK of 34 MPa$\sqrt{m}$. 25200X, TEM.

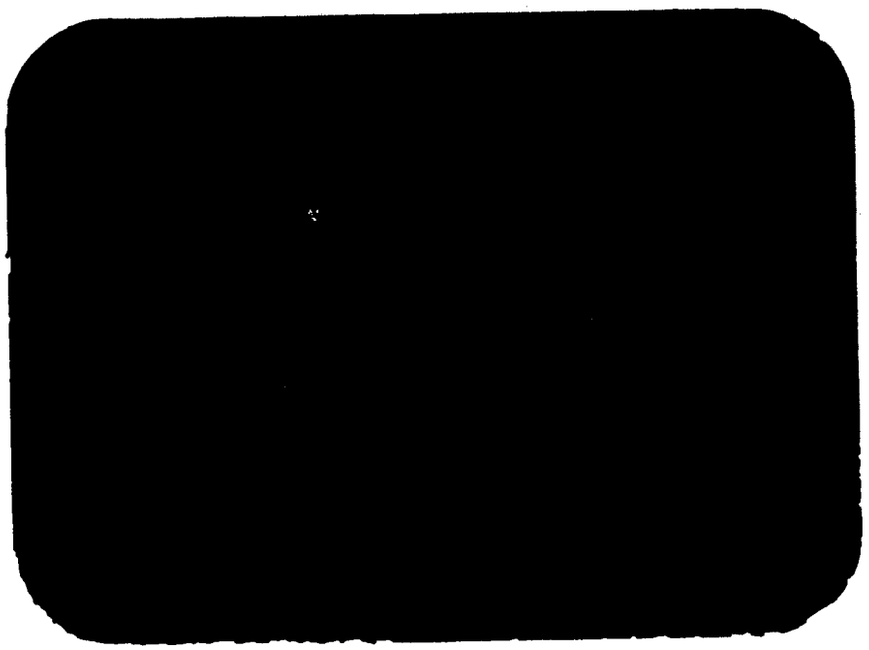

Fig.28 Pearlite boundary failure and ferrite-ferrite intergranular failure on sample A2-54 at an applied ΔK of 34 MPa$\sqrt{m}$. 32640X, TEM.

Fig.29 Severe abrasion and fretting corrosion products typical of all high block-low block specimens. 5000X,SEM.

intensity expression. This would appear to be the case for 2c<t (where 2c = crack width and t = specimen thickness). Until 2c=t, the standard CT stress intensity formulation does not properly express the stress intensity condition at the crack tip. A more useful approach to describe the local stress intensity level should involve the assumption of a semi-elliptical surface flaw at the notch root. The problem is still extremely complicated due to the stress gradient associated with the notch. In addition, one is tempted to use linear elastic fracture mechanics in an area affected by plasticity. Any calculations of propagation life under these conditions would be highly suspect and of little real value.

SEM Examination

The scanning electron microscope, while not allowing the extremely high magnification available from the TEM, is an extremely useful tool. The addition of an x-ray microprobe allows for qualitative chemical analysis of small fracture surface features. Several important observations concerning crack initiation in VAN-80 were made possible by the use of these instruments.

Figure 29 is a SEM photomicrograph of a typical area within the visually determined plastic zone (Figs. 22b & 23b). The surface is covered with abrasion and what is believed to be fretting corrosion products throughout the macroscopically discolored area. Both features

would be due to crack closure effects resulting from compressive residual stresses induced by the high block load. Due to the abrasion, other fracture surface features are wiped out.

In contrast to the severely abraded fracture surfaces described above, fracture surfaces generated during base-line data collection showed little abrasion. On these samples, the crack initiation site or sites could be easily determined due to radial markings emanating from each origin (Figures 30, 31, 32). In every case, these radial markings led to a single particle located at the surface of the notch. In multiple origin specimens, each individual origin contained a particle. A single initiation site sample is shown in Figure 33, the particle being found at the intersection of the radial markings shown previously in Figure 30. Likewise for a multiple origin specimen, Figures 34 and 35 pinpoint the particles at the origins denoted by Figures 31 and 32 respectively. The same sample contained three other origins, one of which is shown in Figure 36. The microproble revealed that each particle consisted of cerium and sulfur; little iron or manganese was found. Thus, the globular cerium sulfides act as crack initiation sites. This is very similar to the findings of Lankford[25] with regard to calcium aluminate inclusions serving as crack initiation sites in 4340 steel. This finding is

Fig. 30 Radial markings emanating from single origin on sample A2-144. 250X, SEM.

Fig. 31 Radial markings issuing from one of five origins on sample A2-95. 300X, SEM.

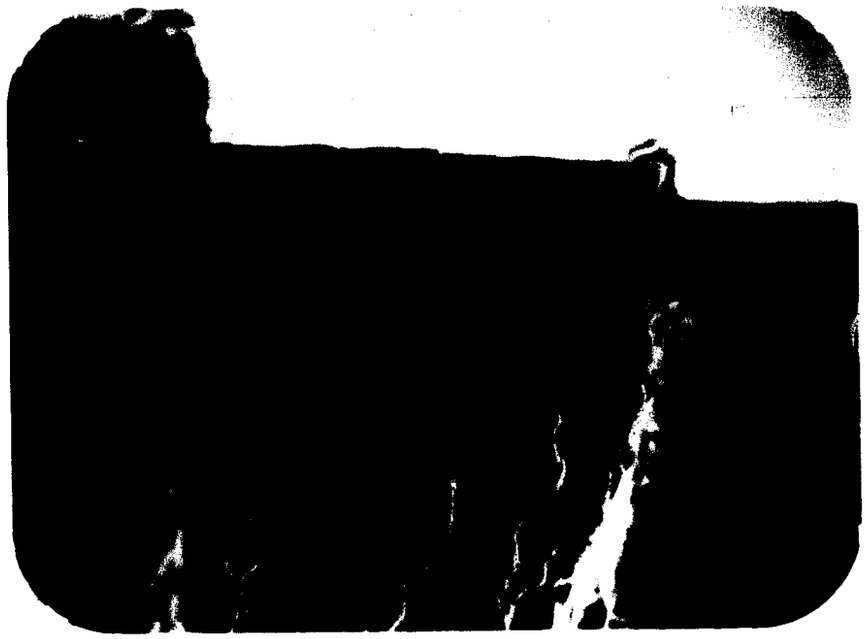

Fig.32 Another one of the five origins on A2-95. Radial markings are evident along with three separate fracture planes. 300X, SEM.

Fig.33 Cerium sulfide at crack origin of sample A2-144. Origin determined by tracing radial markings of Fig. 30. 10000X, SEM.

Fig. 34 Cerium sulfide at the crack origin in A2-95 denoted by radial markings in Fig. 31 6000X, SEM.

Fig. 35 Cerium sulfide at the crack origin in A2-95 denoted by radial markings in Fig. 32 11500X, SEM.

Fig. 36 Cerium sulfide at still another crack origin in sample A2-95. 2125X, SEM.

also significant in another respect. Initiation at sulfide inclusions suggests that the specimen notch polishing procedure was indeed sufficient to remove surface finish as a cause of initiation.

A logical definition for crack initiation is now suggested. The sulfides observed in this Investigation had an average diameter of 1.1×10^{-2} mm. If a method can be found to reliably detect a crack of this size, a workable definition of initiation would exist. It may then be possible to determine the relative importance of initiation and propagation in the formation of a crack of engineering importance.

IV. CONCLUSIONS

Based on the experimental results obtained in this investigation, the following conclusions are presented:

1. The isotropy, which characterizes VAN-80's tensile properties due to inclusion shape control, is also evident in the fatigue crack propagation behavior of this material. For all practical purposes crack propagation rates when loaded longitudinal and transverse to the rolling direction are identical. In spite of VAN-80's high yield strength, fine grain size, and inclusion shape control, crack propagation rates in this material can be described by the same general equation used for normal ferrite-pearlite steels when tested in the L-T orientation.

2. VAN-80 exhibits a fatigue fracture mechanism transition at intermediate stress intensity levels (14-20MPa$\sqrt{m}$). This transition is characterized by a change from structure sensitive crack propagation (as evidenced by intergranular failure) at low ΔK levels to structure insensitive crack propagation (characterized by striation formation) at higher ΔK levels. Fractography can thus help to establish effective ΔK values with or without the presence of striations. The contention by other authors that this transition occurs at a point where a 1:1 ratio exists between grain size and reversed plastic zone size did not hold true for VAN-80.

This may be due to the extremely small grain size found in this material.

3. Data concerning crack initiation from notches of finite radii can be normalized through the application of the parameter $\frac{\Delta K}{\sqrt{\rho}}$. $\frac{\Delta K}{\sqrt{\rho}}$) TH at one million cycles is 835 MPa. Application of data of this type to practical engineering design applications requires the use of elastic-plastic analysis techniques which are beyond the scope of this investigation.

4. A volume effect is seen when analyzing data in terms of $\frac{\Delta K}{\sqrt{\rho}}$. For a given value of $\frac{\Delta K}{\sqrt{\rho}}$ a greater volume of material experiences higher stresses as ρ increases. Consequently, the greater number of potential initiation sites are expected to lead to earlier crack initiation.

5. The results of high block-low block testing where $\Sigma \frac{n}{N} > 1$, seem to indicate that the fatigue process is propagation controlled even for the largest notch radius studied. Since the definition of crack initiation used in this study allows a finite amount of crack propagation (0.25 mm), the answer is not really clear-cut. VAN-80 also exhibits pronounced crack growth rate retardation due to overloads. Consequently, it is still possible that the high block does indeed hasten initiation but that subsequent crack delay due to residual compressive stresses induced by the same initial overloads may be so pronounced that detection of the crack is postponed for very many cycles.

6. TEM fractographic observation has shown that the local effective ΔK level at the tip of short cracks is less than the externally applied ΔK level. Several specimens exhibited the same fracture mechanism transition described in item 2 within the same replica (a distance of approximately 2 mm). Short cracks in the compact tension specimens as a result of crack initiation should therefore be analyzed as semi-elliptical surface flaws. Even so, calculating stress intensity levels at the tips of short cracks becomes difficult due to plasticity considerations.

7. Cerium sulfide particles present at the surface of the notch act as crack initiation sites. Crack initiation in this material can therefore be characterized as the debonding of a sulfide inclusion from the matrix. This suggests that future studies employ this fact as a definition of initiation if suitable detection equipment can be found.

REFERENCES

1. Hertzberg, R. W. and Goodenow, R. H., "Fracture Toughness and Fatigue Crack Propagation in Hot-Rolled Microalloyed Steel," Micro-Alloying 75, Oct. 1975.
2. Jack, A. R. and Price, A. T., "The Initiation of Fatigue Cracks from Notches in Mild Steel Plates", Int. Journ. of Fracture Mech., 6 (1970), pp. 401-409.
3. Barsom, J. M. and McNicol, R. C., "Effect of Stress Concentration on Fatigue-Crack Initiation in HY-130 Steel", ASTM STP559, 1974, pp. 183-204.
4. Clark, W. G. Jr., "Evaluation of the Fatigue Crack Initiation Properties of Type 403 Stainless Steel in Air and Steam Environments", ASTM STP559, 1974, pp. 205-234.
5. Forman, R. G., "Study of Fatigue Crack Initiation from Flaws Using Fracture Mechanics Theory", Engineering Fracture Mechanics, 1972, vol. 4, pp. 333-345.
6. Mattos, R. J. and Lawrence, F. V., "Estimation of the Fatigue Crack Initiation Life in Welds Using Low Cycle Fatigue Concepts", FCP Report #10, The University of Illinois, 1975.
7. Richards, C. E. and Lindley, T. C., "The Influence of Stress Intensity and Microstructure on Fatigue Crack Propagation in Ferritic Materials", Engineering Fracture Mechanics, 1972, vol. 4, pp. 951-978.

8. Birkbeck, G., et. al., "Aspects of Stage II Fatigue Crack Propagation in Low-Carbon Steel", Journal of Materials Science, 6, 1971, pp. 319-323.

9. Cooke, R. J., et.al., "The Slow Fatigue Crack Growth and Threshold Behaviour of a Medium Carbon Alloy Steel in Air and Vacuum", Engineering Fracture Mechanics, 1975, vol. 7, pp. 69-77.

10. Ritchie, R. O. and Knott, J. F., "Mechanisms of Fatigue Crack Growth in Low Alloy Steel", Acta Met., vol. 21, 1973, pp. 639-648.

11. Waldron, G. W. J., et.al., "Application of SEM to the Study of Surface Topography of Fatigue Fractures", Proceedings of the 3rd Annual SEM Symposium, 1970, pp. 297-304.

12. Hertzberg, R. W. and Mills, W. J., "Character of Fatigue Fracture Surface Micromorphology in the Ultra-Low Growth Rate Regime", ASTM STP600, 1976, pp. 220-234.

13. Rolfe, S. T. and Barsom, J. M., Fracture and Fatigue Control in Structures, Prentice-Hall, Englewood Cliffs, New Jersey, 1977, pp. 208-231.

14. Hertzberg, R. W., Deformation and Fracture Mechanics of Engineering Materials, John Wiley, New York, 1976, p. 482.

15. Bates, R. C., and Clark, W. G. Jr., Trans. Quart., ASM, vol. 62, #2, 1969, pp. 380.

16. Miner, M. A., Metal Fatigue, McGraw-Hill, 1959,p.278.

17. Hudson, C. M. and Hardrath, H. F., NASA Tech. Note D-1803, 1963.

18. Schijve, J. and Brock, D., Aircraft Engineering, 34, 1962, p. 314.

19. von Euw, E. F. J., et.al., "Delay Effects in Fatigue Crack Propagation", ASTM STP513, 1972, p. 230.

20. Trebules, V. W., et.al., Effect of Multiple Overloads on Fatigue Crack Propagation in 2024-T3 Aluminum Alloy", ASTM STP 536, 1973, p. 115.

21. Mills, W. J., et.al., "Load Interaction Effects on Fatigue Crack Growth in A514F Steel Alloy.

22. Roberts, R. and Hertzberg, R. W., PSEF Proposal, 1976.

23. Braglia, B. L., Fatigue Resistance of Fillet Welds, BS Thesis, General Motors Institute, 1975.

24. Creager, M. The Elastic Stress-Field Near the Tip of a Blunt Crack, MS Thesis, Lehigh University, 1966.

25. Lankford, J., "Inclusion-Matrix Debonding and Fatigue Crack Initiation in Low Alloy Steel", Int. Journal of Fracture, 12, 1976, pp. 155-157.

VITA

Brian Lee Braglia was born in a suburban Chicago hospital on August 31, 1952, to parents Bruno and Stella Braglia. Upon graduation from Mendel High School in Chicago he entered the Mechanical Engineering program at General Motors Institute in Flint, Michigan. All students at GMI participate in a cooperative work-study program which allows them to acquire theoretical knowledge of their chosen field at GMI and practical experience at a sponsoring General Motors unit. Work periods during the first three years were spent at the GM Research Laboratories. At the end of his junior year he transferred to the Engineering Department of GM's Electro-Motive Division where he spent the remainder of the cooperative phase in the Materials Laboratory. His undergraduate thesis, Fatigue Resistance of Fillet Welds, examined crack initiation in fillet welds and the effects of non-intentional defects on crack initiation life.

While at GMI, he was elected to the honorary engineering fraternity Tau Beta Pi and was named to the Dean's List every semester. While still a freshman he joined Beta Theta Pi fraternity and eventually served as secretary, treasurer, and finally presiding officer of the Delta Eta chapter.

Upon graduation from GMI in February, 1975, he continued work as a metallurgist at EMD for several months. He then became EMD Engineering Representative to the Southern Pacific Railroad with the title of Field Project Engineer. Upon expiration of the one year assignment he returned to the Materials Lab as a metallurgist before taking a one year educational leave of absence for graduate study at Lehigh under the GM Fellowship Plan.

At Lehigh he became a very active member of the esteemed von Laue Scoiety. As starting pitcher for the department softball team he compiled a record of 8-5 with an ERA of 1.49 which isn't bad considering this was a slow-pitch league.